

5

Application of Extreme Models

Physicists always have a habit of taking the simplest example of any phenomenon and calling it “physics”, leaving the more complicated examples to become the concern of other fields—say, of applied mathematics, electrical engineering, chemistry, or crystallography.

“The Feynman lectures on physics”

5.1. Thermodynamics of Atmosphere

Objectives of Study

This section and, indeed, whole chapter are offered to illustrate the use of *extreme thermodynamic models* in applied problems, on the one hand, and to reveal the difficulties arising from such model’s application. We also consider methods eliminating these difficulties.

Capabilities of thermodynamic modeling can be shown by the detailed description of the inferences of modeling, explanation of their originality, formulation complexity without using thermodynamics principles, usefulness for understanding the studied process nature, and elaboration of measures for its improvement.

Presentation of the problems of applying these models implies disclosure of secrets of their construction regarding specific features of the object under study; description of computational experiments on their basis and application of other models in these experiments and information collected from different sources.

Why is it interesting to analyze air pollution processes to exemplify and illustrate the capabilities of extreme thermodynamic modeling? There are several reasons.

First of all, *chemical processes in the atmosphere proceed at low temperatures* in comparison with the majority of technological and many other natural processes. Except for photochemical transformations, they are also characterized by extremely low rates and do not reach a final equilibrium point (see Section 1.4). Live nature and harmful anthropogenic substances in the atmosphere are in partial equilibrium states. This helps explain the skepticism of many specialists concerning possible application of thermodynamics to atmospheric chemistry. In terms of

development of applied thermodynamics and choice of models to study pollution of the atmosphere and the environment as a whole, it is highly important that we explain invalidity of such skepticism, doing so by using examples of problems that were earlier considered beyond the sphere of thermodynamic analysis.

The next reason to study the air pollution with the help of MEIS is associated with the *complexity of the atmosphere as a thermodynamic system*. “Complexity” in this case means both a great number of variables influence the values of thermodynamic functions, and the corresponding mathematical model is complex with respect to its construction, our analysis of its specific features, and the execution of numerical experiments on its basis.

The atmosphere is an open heterogeneous system that interacts with the nonequilibrium environment. It comprises a gas phase, as well as water droplets and aerosols (solid and liquid, anthropogenic and natural) [36, 166]. The latter can be pure condensed substances, but more often they have a heterogeneous spatially non-uniform structure, in particular, they are solutions on the surface of solid particles. Both gaseous and condensed matter of the atmosphere is distributed unevenly with respect to height (mainly due to decrease of air density with height) and on the horizontal plane (because of air flow).

The nonequilibrium nature of the environment is conditioned by the difference of temperatures between the aquatic and terrestrial surfaces and radiation (solar and reflected), and also by pressure variation in horizontal direction under the influence of heat and mass transfer.

The composition and spatial distribution of substances change in response to highly diverse physical forces, including chemical affinity, gravity, wind pressure, surface tension, electrical interactions, and others. The transfer processes of energy, substance, and charge that are caused by these forces are often characterized by pronounced irreversibility and have in some cases a clearly defined nonstationary character.

Successful qualitative and quantitative analysis of such a complex system as the atmosphere using rather simple models is surely the best demonstration of the competence and efficiency of thermodynamic idealization of a problem.

Unfortunately, this interest has also been generated by great *practical* significance of the problem. Air pollution is known to be a major part of the bigger problem of maintaining life on Earth.

Finally, this example is interesting because the anthropogenic impact on the atmosphere is the subject of very extensive studies on theoretical models and full-scale experiments. And though the results of these studies do not allow a unique assessment of the consequences of our current influence on nature, they provide rich material for the analysis of thermodynamic modeling results. The information obtained by nonthermodynamic models and measurements of real atmospheric states can be used to check correctness of thermodynamic methods for solving similar problems, and to set up schemes for their joint application with kinetic and hydrodynamic models in computational experiments.

We will address three particular problems within the general problem of atmosphere thermodynamics: 1) assessment of the limiting concentrations of water

vapor; 2) determination of relationships between concentrations of primary and secondary pollutants; 3) determination of distribution of harmful substances in a vertical air column.

Assessment of Limiting Concentrations of Water Vapor

As distinct from the two following problems and most of the problems on atmospheric chemistry, this one is traditionally described in terms of thermodynamics. The section entitled “Humid Air” is commonly included in manuals on technical thermodynamics and heat engineering (see, for example, [114]). However, the air humidity dependence on temperature and enthalpy is analyzed in them on the basis of the simplest relations assuming that pressure is constant and there is no impact of microcomponents contained in the atmosphere on concentration and phase state of water.

MEIS-based studies for different combinations of T and P have shown first of all the correctness of the applied mathematical descriptions. Discrepancy between the results by the known L.K. Ramzin’s Id-diagram (enthalpy vs. moisture content) and the data of full-scale measurements in [25] was no more than 0.5%. A variant of calculations is given in Table 5.1.

Note that the calculations were performed on the model of the ideal gas phase. In this case the parameters of the modeled system at the points located on the curve of phase transitions (gas-to-liquid) were determined with high accuracy. Though such an excellent result of calculations is easily explained by the very low partial pressure of saturated water vapor, the considered fact expands our understanding of the capabilities of ideal models (with a logarithmic nature of change in the values of thermodynamic functions at deviation of parameters from the standard values). For comparison the last column of the table contains the results of similar calculations regarding the real sizes of water droplets, i.e., regarding the surface tension for the condensed phase. The value of $x_{\text{H}_2\text{O}(c)}^{\text{eq}}$ in the example is seen to change considerably (by 4.6%), and this should be borne in mind in the analysis of atmospheric processes.

TABLE 5.1. Calculation of the limiting concentration of water vapor in the atmosphere ($T = 293.15$ K, $P = 98.0$ kPa)

Substance	State, mole		
	y	$x^{\text{eq}}(r_{\text{H}_2\text{O}} \rightarrow \infty)$	$x^{\text{eq}}(r_{\text{H}_2\text{O}} = 0.1 \mu\text{m})$
Ar	0.93	0.93	0.93
N ₂	78.08	78.08	78.08
O ₂	20.95	20.95	20.95
CO ₂	0.03	0.03	0.03
NO	0.00	$1.0 \cdot 10^{-14}$	$1.0 \cdot 10^{-14}$
NO ₂	0.00	$1.0 \cdot 10^{-8}$	$1.0 \cdot 10^{-8}$
H ₂ O _(g)	0.00	2.35	2.38
H ₂ O _(c)	3.00	0.65	0.62

Practical significance of the problem of searching for $x_{\text{H}_2\text{O}(\text{g})}^{\text{eq}}$ is dictated by the fact that only its solution will make it possible to determine conditions for forming fogs, smog, and acid rain [133]. A lot of harmful substances are formed in water solutions, namely on the surface of aerosols, rain droplets, haze and fog [36, 159]. Thermodynamic modeling allows estimation of the impact of anthropogenic change in chemical composition of the atmosphere in industrial centers on water film formation around aerosols, mist formation, composition of rudimentary germ drops, content of secondary pollutants in them, and, finally, air quality and climate of a city. It should be stressed that drops of fog and clouds appearing at humidity close to 100% are usually very diluted solutions and the effect of solution composition and drop radius on the maximum content of water vapor above them is on the whole negligible [15, 36]. The flooding of aerosols is known to start at relative humidity (f) equal to around 30% and to lead to variation in the optical characteristics of the atmosphere. On the average haze appears at a relative humidity of about 80% [179]. Haze drops are just a diluted solution of electrolytes, however, the solution composition still influences essentially a condensation process. Therefore, the calculated composition of a haze droplet is given as an example. Table 5.2 gives an indication of the possible “harmfulness” of solution. Its data were obtained on the basis of high idealization of real phenomena. The sorption processes, for example, were not dealt with at all. The action of surface tension forces was taken into consideration approximately, i.e., by making adjustments calculated for the fixed radii of particles. The calculation results are given for both the condensed phase evenly distributed in some volume of the atmosphere ($r \rightarrow \infty$) and drops with the radius $r = 0.1 \mu\text{m}$ (10^{-7} m). Since the available model describes in principle only diluted solutions, changes in the surface tension are considered solely for water.

However, despite some simplifications the model of liquid phase aerosol qualitatively correctly simulates the processes of equilibrium heterogeneous condensation in the real atmosphere [119].

In particular, change in the concentration of electrolyte solution with decrease in the relative humidity of air is determined within a sufficient range of accuracy (Fig. 5.1). The results for different initial compositions (0.5 of AQS¹ NO₂ and 5

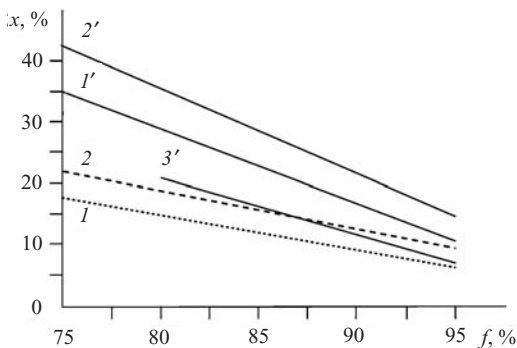


FIGURE 5.1. Change in the total concentration of ions in a drop with an increase of relative humidity ($T = 298$ K). 1, 2 – calculation results, 1', 2', and 3' – published data.

TABLE 5.2. Modeling results of the liquid phase aerosol in the atmosphere
 ($T = 298\text{K}$, $f = 99\%$, $P = 1\text{ atm}$)

Substance	$G_0(r \rightarrow \infty)$, J/mole,	y , mole/kg	$x^{\text{eq}}(r_{\text{H}_2\text{O}} \rightarrow \infty)$, mole/kg	$x^{\text{eq}}(r_{\text{H}_2\text{O}} = 0.1\mu\text{m})$, mole/kg
<i>Gas phase</i>				
HNO ₃	-213410	$5.11 \cdot 10^{-8}$	$7.22 \cdot 10^{-12}$	$5.83 \cdot 10^{-12}$
H ₂ O ₂	-205732	$6.55 \cdot 10^{-9}$	$4.35 \cdot 10^{-16}$	$1.16 \cdot 10^{-16}$
O ₃	70613.5	$1.42 \cdot 10^{-6}$	0.0	0.0
O ₂	-61110	7.18	7.16	7.16
NO ₂	-37345.4	$4.58 \cdot 10^{-7}$	$1.44 \cdot 10^{-11}$	$3.89 \cdot 10^{-12}$
NO	28486.8	$6.06 \cdot 10^{-12}$	$4.62 \cdot 10^{-10}$	$1.24 \cdot 10^{-12}$
N ₂ O ₅	-92682	$2.91 \cdot 10^{-10}$	0.0	0.0
HNO ₂	-154133	$7.88 \cdot 10^{-13}$	$1.16 \cdot 10^{-10}$	$3.11 \cdot 10^{-11}$
CO	-169407	$7.11 \cdot 10^{-6}$	0.0	0.0
H ₂	-38904.9	$1.96 \cdot 10^{-5}$	0.0	0.0
N ₂	-57071.6	26.7	26.7	26.7
H ₂ O	-298051	1.03	1.04	1.04
CH ₄	-130107	$6.13 \cdot 10^{-3}$	$1.28 \cdot 10^{-17}$	$3.44 \cdot 10^{-18}$
CO ₂	-457182	$1.19 \cdot 10^{-2}$	$1.80 \cdot 10^{-2}$	$1.80 \cdot 10^{-2}$
C ₂ H ₄	-12921.6	$1.74 \cdot 10^{-9}$	0.0	0.0
C ₃ H ₆	-59130.2	$1.87 \cdot 10^{-9}$	0.0	0.0
SO ₂	-370743	$6.55 \cdot 10^{-7}$	$4.64 \cdot 10^{-12}$	$1.25 \cdot 10^{-9}$
CH ₃ Cl	-151824	$3.50 \cdot 10^{-7}$	0.0	0.0
HCl	-147978	0.0	$2.05 \cdot 10^{-8}$	$1.41 \cdot 10^{-9}$
<i>Solution</i>				
H ₂ O _(c)	-306714	$3.50 \cdot 10^{-5}$	$5.16 \cdot 10^{-4}$	$1.45 \cdot 10^{-4}$
H ⁺ NO ₃ ⁻	-243873	$3.50 \cdot 10^{-14}$	$1.25 \cdot 10^{-7}$	$1.36 \cdot 10^{-7}$
H ⁺ HCO ₃ ⁻	-713359	$3.50 \cdot 10^{-14}$	$1.28 \cdot 10^{-7}$	$3.44 \cdot 10^{-8}$
H ₂ SO ₄ ⁺	-1800384	$3.50 \cdot 10^{-14}$	$6.55 \cdot 10^{-7}$	$6.55 \cdot 10^{-7}$
H ⁺ Cl ⁻	-177537	$3.50 \cdot 10^{-14}$	$3.30 \cdot 10^{-7}$	$3.49 \cdot 10^{-7}$
M, kg	—	0.0286	0.0286	0.0286
G, J	—	-66641.1	-66782.3	-66782.3
Ionic strength	—	—	$2.74 \cdot 10^{-1}$	$9.48 \cdot 10^{-1}$

of AQS of NO₂ at a gas phase) that were obtained by the authors on the model of solutions are under 1 and 2; the curves 1', 2', 3' [119] are the published data for different compositions of components of the liquid-phase aerosol, respectively for the background conditions, polluted atmosphere and laboratory model representing a mixture of dry air and NaCl solution.

As distinct from other models, thermodynamic modeling makes it possible to vary a composition of gaseous pollutants and components of the electrolyte solution over a wide range. As a result the relationship between concentrations of different solution components, the limiting content of water vapor directly in the drop vicinity, and correspondingly the drop sizes can be determined. Besides, it becomes

¹ Here the value of the Russian national air quality standard (AQS) is used as a unit of concentration

feasible to study the effect of the initial concentration of gaseous pollutants on solution composition as well as absorptive capacities of drops with different radii.

The thermodynamic models of change in air humidity are to be applied to the study of atmospheric pollution processes and to calculate air conditioning systems and different-purpose drying installations. In this case, unlike the use of diagrams, we can vary parameters of air composition or drying agent (the latter may contain products of fuel combustion). The topicality of thermodynamic modeling of air exchange in buildings was shown in Section 3.4.

Analysis of Secondary Atmospheric Pollution

This problem refers to the “illicit” sphere of thermodynamics application, since in the final equilibrium state the concentrations of the majority of known pollutants turn out to be some orders of magnitude lower than the admissible ones and are practically equal to zero, which does not correspond to reality.

Solving the problem requires that we overcome certain numerical difficulties. One of them, i.e., a wide scatter in the values of sought parameters, was discussed in Section 4.3. Another one consists in a great number of primary and secondary pollutants and dependence of their conversion reactions in the atmosphere on several factors (temperature, air pressure and humidity, solar radiation, etc.). Determination of dependences in formation of many pollutants on different parameters naturally gives rise to the problem of reducing the number of calculation variants, i.e., the problem of conducting computational experiments. Therefore, the secondary pollution problem should be discussed starting with the technique of studies to be performed.

Its basic point is certainly the choice of an initial thermodynamic model. In this case a closed spatially uniform heterogeneous system with a fixed initial composition of reagents that interacts with the environment at the constant T and P was considered. The premise on the system closedness is equivalent to the assumption that all processes manage to reach the states of partial or complete equilibria. The spatial uniformity means that surface tension forces at phase transitions are neglected. Assumption of constant temperature and pressure limits the analysis to a ground layer of the atmosphere, whose pollution is the most dangerous for nature and humans. With these assumptions made the mathematical formulation of the problem is apparently reduced to the simplest MEIS modification, i.e., (2.38)–(2.42).

A natural way to decrease the volume of computational experiments is to make a small number of calculations of some typical states and to extend their results to other possible states based on the simplest analytical dependences. Such dependences can be determined from the fact that since the atmosphere is an oxidizing medium, the danger of primary emissions in terms of secondary pollution of the atmosphere is caused to a considerable extent by their reactivity in oxidization processes. Indeed, the energy necessary to drive the reaction of secondary pollutant formation may come only from the reactions of primary pollutant oxidation. As far as we consider the system with the constant T and P , the concentration of

the j th secondary pollutant changes directly as a function of change in *Gibbs energy surface shape of the system* (ΔG) due to increase (decrease) in concentration of the p th primary pollutant.

It can be admitted that

$$\Delta G = \Delta G_p^{\text{ox}}, \quad (5.1)$$

where ΔG_p^{ox} is the Gibbs energy change in the oxidization reaction of the p th component; then

$$\Delta G_p^{\text{ox}} = \alpha G_{pO} - \beta G_p - \gamma G_O, \quad (5.2)$$

where α , β and γ are stoichiometric coefficients; the indices pO , p , and O at the values of G refer to the oxidization product, pollutant, and oxygen, respectively.

Since the absolute values and the increases in pollutant concentrations are very small quantities, the following expression seems admissible:

$$x_j^{\text{ext}} - x_j^b = \frac{\Delta G_p^{\text{ox}}}{\left(\partial G_p^{\text{ox}} / \partial x_j^b\right)}, \quad (5.3)$$

where x_j^b is the extreme concentration of the j th secondary pollutant in the background (conventionally clean) atmosphere.

Assuming that the reacting gases are ideal, we have

$$\frac{\partial G_p^{\text{ox}}}{\partial x_j^b} = G_j^0 + RT \ln x_j^b - RT \ln \sigma \approx a' + RT \ln x_j^b, \quad (5.4)$$

since the total quantity of moles σ in the atmosphere is virtually constant.

As the value of x_j^b is given, then

$$x_j^{\text{ext}} - x_j^b = a \Delta G_p^{\text{ox}}. \quad (5.5)$$

The letter a in (5.4), (5.5) and elsewhere in this section denotes constant coefficients.

To interpret relation (5.5) graphically let us consider an idealized system in which the initial reagents are monatomic gases and the reactions result in formation of the monoxide of primary pollutant and the monoxide representing a secondary pollutant. For this system $x = (x_O, x_p, x_j, x_{pO}, x_{pj})^T$ and $y = (y_O, y_p, y_j)^T$. It is easy to apply, because it does not depend on the choice of primary pollutant (p), oxidized component (j) and secondary pollutant (pj), and therefore the material balance polyhedron $D(y)$ does not change and the concentration $x_{pj} = x_{jO}$ is determined only by the thermodynamic properties of the components.

Figure 5.2 represents a two-dimensional face of $D(y)$ whose vertices correspond to the initial mixture composition and the maximum concentrations of oxides of the primary (x_{pO}^{mat}) and the secondary (x_{jO}^{mat}) pollutants. Two surfaces of the Gibbs energy are put over the plane $y - x_{pO} - x_{jO}$. The upper surface (the index s) refers to the system with a low oxidizing capacity of the primary pollutant and the lower surface (the index l)—refers to the system with a large value of ΔG_p^{ox} .

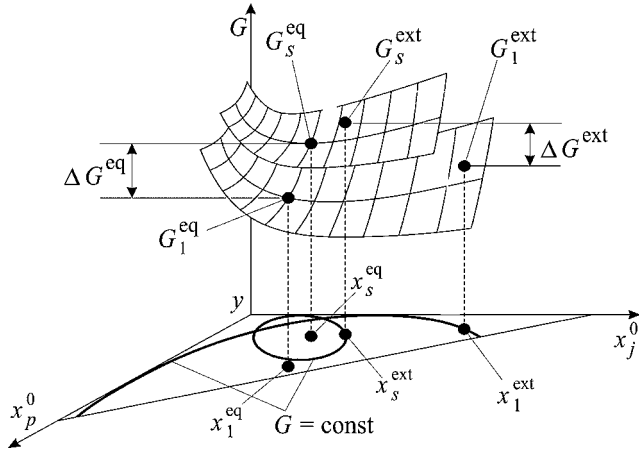


FIGURE 5.2. Graphical interpretation of atmosphere's sensitivity versus oxidizing capacity of the primary pollutant.

Fig. 5.2 shows that moving along the trajectory $y - x_{jO}^{ext}$ we approach closer the vertex x_{jo} and hence, achieve a much higher concentration of the secondary pollutant than when moving along the trajectory $y - x_{jOs}^{ext}$.

However, relation (5.5) is difficult enough to apply to computational experiments despite its simplicity, since

$$\Delta G_p^{ox} = f(A_p^{ox}, \ln x_1, \dots, \ln x_n),$$

where A_p^{ox} is the standard chemical affinity of the oxidation reaction for the p th pollutant. Hence, it is desirable to pass from ΔG_p^{ox} to another function that does not depend on the partial pressures of the reaction mixture components. *Enthalpy* is such a function for ideal gases. Its application in this case proves to be convenient, because at temperatures of Earth's atmosphere, $H_j \gg TS_j$, and it can be admitted that

$$\Delta G_p^{ox} = \Delta H_p^{ox} - \Delta(TS)_p^{ox} \approx \Delta H_p^{ox}. \tag{5.6}$$

Therefore, we can pass from (5.5) to the expression

$$x_j^{ext} - x_j^b = \alpha \Delta H_p^{ox}. \tag{5.7}$$

Application of equation (5.7) sharply decreases the volumes of thermodynamic calculations. In essence it is necessary to calculate the values of extreme concentrations of secondary pollutants in the background atmosphere (x_j^b) by MEIS and to determine the coefficients α based on several calculations.

Some results of computational experiments that are obtained using the linear dependence (5.7) are presented in Figs. 5.3 and 5.4. The values

$$r_{pj} = \frac{x_{pj}^{ext} - x_j^b}{x_j^b} = \frac{\Delta x_{pj}}{x_j^b}, \tag{5.8}$$

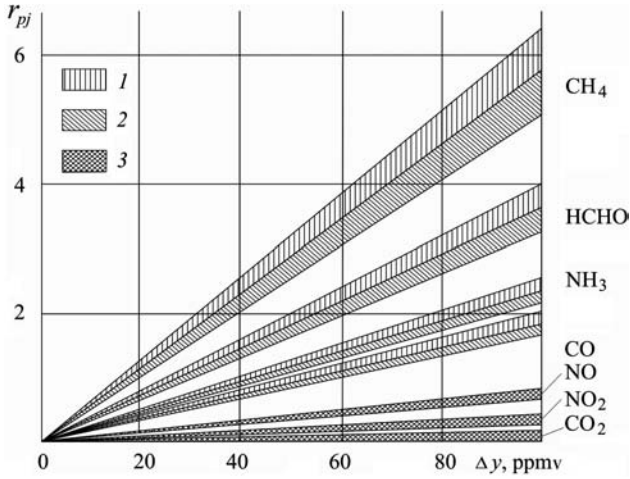


FIGURE 5.3. Relative responses of the atmosphere to emission of particular pollutants (the pollutants are denoted on the right). Secondary pollutants: 1—organic, 2—inorganic, 3—organic and inorganic.

are plotted along the vertical axis in dimensionless units in Fig. 5.3 and can be interpreted as the environmental responses to emissions of the p th pollutant. Figure 5.4 presents the dependence on ΔH_p^{ox} of the value

$$K_{pj} = \frac{\Delta x_{pj}}{y_p} = \frac{r_{pj} x_j^b}{y_p} \tag{5.9}$$

which characterizes the atmosphere's sensitivity to the p th pollutant.

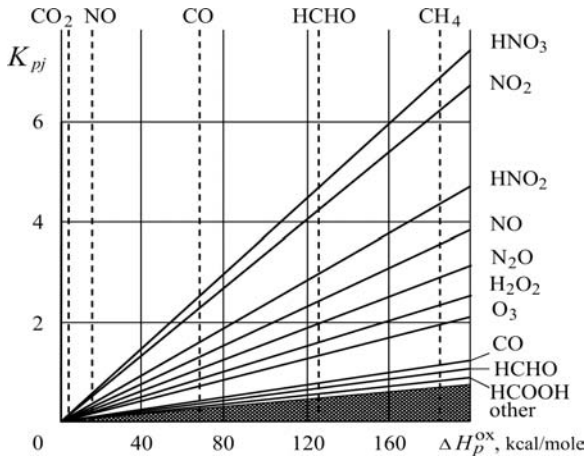


FIGURE 5.4. Coefficients of chemical sensitivity of the atmosphere versus the oxidation heat of primary pollutant.

Figures 5.3 and 5.4 show the effect of oxidation heat of primary pollutants on the secondary pollution of the atmosphere. The highest values of the coefficients K are typical of methane. The conclusions drawn from the thermodynamic analysis on the higher sensitivity of the atmosphere to hydrocarbon emission are in good agreement with the results of kinetic and experimental studies [12, 163, 164, 169].

The danger of secondary environmental pollution is determined both by the relations $\Delta x_{pj}/y_p$ and the relationships between the toxicity of the j th and p th substances. Hence, it does make sense to characterize every primary pollutant by the individual (D_{pj}) and integral (D_p) coefficients of environmental danger:

$$D_{pj} = \frac{\Delta x_{pj}/\text{AQS}_j}{y_p/\text{AQS}_p}, \quad (5.10)$$

$$D_p = \frac{\sum_{j=1}^n (\Delta x_{pj}/\text{AQS}_j)}{n (y_p/\text{AQS}_p)}, \quad (5.11)$$

where AQS_j and AQS_p are the limiting guideline concentrations of the j th and p th substances; and n is the number of considered secondary pollutants.

The coefficients D_{pj} and D_p show how much the formation of the j th secondary pollutant (or the sum of pollutant in the case of D_p) in the atmosphere is more dangerous than that of the initial p th substance. At $D_{pj} > 1$ and $D_p > 1$ the products of transformation processes in the atmosphere are more dangerous than the initial reagents. It is obvious that for the case of emission of several primary pollutants the denominators of formulas (5.10) and (5.11) should contain the sums of their concentrations. Thus, the indices D_{pj} and D_p can characterize in full measure a risk of the secondary pollution of the atmosphere with anthropogenic emissions.

Table 5.3 presents the results of calculating D_{pj} for the most typical components in the energy-related emissions: methane (CH_4), carbon monoxide (CO), formaldehyde (HCOH), nitrogen monoxide (NO) and ammonia (NH_3). The table shows that in many cases the products formed can be more hazardous than the initial substances ($D_{pj} \gg 1$). This pertains first of all to methane emissions. Special attention should be paid to the risk of secondary atmospheric pollution by benzpyrene, ozone, and prussic acid. Even with an error in determination of D_{pj} one or two orders of magnitude, the conclusions drawn are invariable.

Among other things, the results of the presented thermodynamic analysis can be used to specify the directions that the experimental and numerical kinetic studies may take. Kinetics and experiments in turn can help in the formulation of constraints for the further thermodynamic modeling of harmful emission behavior in the atmosphere.

Distribution of Harmful Substances in a Vertical Air Column

Solution to this problem has already been dealt with in Section 2.3 as an illustration of one possible application of MEIS for spatially nonuniform structures. Therefore, here we will limit ourselves to several remarks only.

TABLE 5.3. Average values of the coefficient of additional environmental hazard due to energy-related emissions (D_{pi})

Secondary pollutant		Primary emissions				
		CH ₄	CO	HCHO	NO	NH ₃
Ozone	O ₃	13000	280	13	300	180
Carbon monoxide	CO	34	0.8	0.5	0	0.5
Hydrogen peroxide	H ₂ O ₂	1200	20	1.3	33	13
Nitrogen oxide	NO	100	2.2	0.1	1.2	1.5
Nitrogen dioxide	NO ₂	2500	36	2.3	47	13
Dinitrogen oxide	N ₂ O	450	8.6	0.4	7.0	7.5
Ammonia	NH ₃	30	0.5	0	0.5	0.6
Nitric acid	HNO ₃	1100	37	1.1	22	9.4
Prussic acid	HCN	1100	28	1.3	37	14
Hydrazine	N ₂ H ₄	4300	46	5.1	63	47
Formaldehyde	HCOH	810	18	0.9	17	8.3
Formic acid	HCOOH	630	19	0.6	17	8.9
Acetaldehyde	CH ₃ COH	40	0.8	10	1.0	0.5
Acetic acid	CH ₃ COOH	56	1.3	0.1	1.0	0.7
Ethylene	C ₂ H ₄	1.7	0	0	0.1	0
Butadiene-1,3	C ₄ H ₆	1.0	0	0	0	0
Acetone	CH ₃ COCH ₃	0.7	0	0	0	0
Methanol	CH ₃ OH	63	0.5	0.1	1.2	1.0
Benzene	C ₆ H ₆	4.7	0.1	0	0.1	0
Toluene	CH ₃ C ₆ H ₅	1.4	0	0	0	0
Phenol	C ₆ H ₅ OH	240	3.6	0.3	5.2	1.2
Ethyl benzene	C ₆ H ₅ C ₂ H ₅	1.1	0	0	0	0
Pyridine	C ₅ H ₅ N	18	0.3	0	0.4	0.1
Ethylamine	C ₂ H ₅ N	8	0.1	0.1	0.1	0.1
Naphthalene	C ₁₀ H ₈	0	0	0	0.1	0
Phenanthrene	C ₁₄ H ₁₀	0.5	1.2	0.1	0.8	0.3
Benzpyrene	C ₂₀ H ₁₂	150000	3600	210	3200	1900

The first of them elucidates the given problem in the literature. The data that are theoretically justified by the Boltzmann distribution and confirmed experimentally concern only basic macrocomponents of the atmosphere (N₂, O₂, Ar, CO₂). The theoretical analysis was limited to consideration of the only force—gravity. Distribution of microcomponents was studied solely for individual substances, for example ozone, whose concentrations in the upper and lower atmospheric layers have different effects on the environmental state.

The general model for distribution of gaseous microcomponents and aerosols in the vertical air column with an account for their chemical transformations and phase transitions and the effects of different forces is certainly interesting from both the theoretical and applied standpoints. Of special concern is a nonisothermal model of the atmosphere that would help us study formation of cloudy and aerosol layers in the stratosphere, where processes are relatively stable in comparison to the lower layers. The concentration of pollutants in lower layers is determined primarily by the intensity of turbulent motion of a different scale. In the last decade the problems of possible human-induced impact on the global climate has become

extremely topical. An important aspect of the problem is to assess a role of the troposphere and stratospheric aerosol in the processes of scatter and reflection of short- and long-wave radiation and also condensation, i.e., formation of the cloud cover [1]. The most difficult problem here is determining the contribution of anthropogenic particles or the indirect human-induced effect on aerosol formation and transfer and on atmospheric chemistry in general [11]. The thermodynamic model of the vertical air column would possibly assist in revealing some laws concerning specific features in formation of the aerosol layers regarding their dispersion and chemical composition.

Depending on the objectives of the study, the thermodynamic modeling can examine different column heights at different steps in the vertical plane. Variation of the sizes and structure of cells in the modeled system provides an idea of both distribution of harmful substances in the ground layer of the atmosphere (under certain conditions) and processes extending over the whole column of the troposphere and even in the middle atmosphere.

It was shown in [92] that MEIS for spatially inhomogeneous structures could be applied to the analysis of substance distribution over the horizontal plane as well. In this case, terrain relief and other factors can be taken into consideration.

Application of spatial thermodynamic models in combination with models of chemical kinetics and *transfer* (motion induced by pressure drop, molecular and turbulent diffusion, heat exchange) proves to be the most effective. Increase in the number of quite different models to describe one and the same system we may suppose will give a deeper insight into the processes occurring in that system and lead to accurate forecasting of processes' results.

5.2. Thermodynamics of Combustion

Introductory Notes

Unlike atmospheric chemistry, the chemistry of combustion was not a forbidden area for thermodynamic analysis. As was mentioned in the Introduction (Section I.23), the main features of hydrogen combustion thermodynamics were discovered by D. Gibbs. Now the thermodynamic interpretations of oxidation of the main combustible components in fossil fuel are clear. However, currently, environmental characteristics of furnaces and combustion chambers are studied almost solely by kinetic models and full-scale experiments. And the necessity for thermodynamic methods to penetrate into this sphere of studies has yet to be demonstrated. In this section of the book the authors make one more attempt (the previous ones are presented, e.g., in [50, 80, 81]) to explain a certain technique of using thermodynamic models and reveal the model's effectiveness for the analysis of harmful substances formed at fuel burning.

In terms of revealing the capabilities of thermodynamics, the processes of both combustion and atmospheric pollution are highly interesting because of their complexity and great practical significance. Besides, the available abundant data on

release of pollutants during fuel burning allows the estimation of thermodynamic modeling accuracy and facilitates elaboration of algorithms of joint application of the kinetic and thermodynamic models and full-scale experiments to study physicochemical processes. We now describe the factors determining the scientific significance of combustion thermodynamics in greater detail.

Fuel is burnt in open systems with a nonequilibrium environment. Mass is exchanged with the latter by flows of fuel, air (oxidant), recirculating and flue gases, slag, and ash of different temperature. As a rule these systems are heterogeneous. Heterogeneity proves to be highest at solid fuel combustion, first among these being coals that consist of both organic and diverse mineral matter. Reactions with participation of the mineral part of fuel can result in formation of gaseous and condensed compounds. The number of reaction mixture components may reach many hundreds. Design of a combustion appliance and the arrangement of fuel burning in it stipulate both chemical and other interactions: mechanical, thermal, gravitational, electrical and electromagnetic, and radiative.

Periodic processes of fuel combustion at small boiler plants and furnaces are not steady. However, steadiness is most typical of operation of transport engines. A revelation of the specific features of such complex real objects by comparatively simple models of equilibria seems highly instructive to the task of mastering the art of thermodynamic modeling.

The practical importance of environmental analysis of fuel combustion processes, it being a key source of pollution in nature, requires no comment. Thermodynamics, however, allows both estimation of the potential negative impact of production installations on the environment and determination of the factors influencing the reliability and security of equipment operation. Thermodynamic studies on slag formation at water pipes of furnaces, as well as sulfuric acid corrosion of the rear heating surfaces of boiler units, are examples of problems related to the reliability problem. We may recall the practical significance of such traditional thermodynamic analysis applied in the energy sector for determining specific fuel consumption for production processes.

Combustion is a better illustration than atmospheric pollution, when we tend to compare thermodynamic models to kinetic models and full-scale experiments. In human-organized processes as compared to natural ones, it is much easier to determine initial system state, conditions of interaction with the environment, and possible ranges of initial data variation. When we study atmospheric pollution it turns out to be rather difficult to estimate composition prior to anthropogenic impacts and the extent of these impacts (emissions of harmful substances). It is extremely difficult to take into account the effect of infinitely diverse natural factors (solar radiation, air flows, mass exchange with water and ground surfaces, etc.) on all the microcomponents present in the atmosphere.

A wide experience has been gained by now on MEIS application to the analysis of combustion processes for different types of coals, heavy oil, gas, production waste, designs of boiler furnaces and stoves, and furnace regimes. Environmental characteristics of energy and public utility installations for fuel combustion have been studied to the greatest extent [50, 81, 138]. Nonequilibrium

plasma ignition and lightening of pulverized-coal torches have been also analyzed.

Here we will dwell on only two problems: 1) analysis of nitrogen oxide formation at coal combustion; and 2) study of the environmental characteristics of periodic processes of solid fuel combustion at small boiler plants and stoves.

Theoretically interesting issues of MEIS application to the study of nonequilibrium plasma processes are considered briefly in the next section.

Thermodynamic Modeling of Nitrogen Oxides Formation in Coal Furnaces

The processes of NO_x formation at fuel combustion have long been the subject of systematic studies for many specialists in different countries [48, 147, 165, 169, 176]. Such studies resulted in accumulation of a wide range of experimental data. There are theoretical achievements and practical recommendations, and many of them have already been implemented. However, many problems call for further investigation in this sphere. They are, for example, raising the efficiency of technologies for NO_x emission reduction, evaluation of the potential for improving these technologies, prevention from formation of other harmful substances due to NO_x suppression, and so on.

MEIS was used for the thermodynamic analysis of forming thermal, fuel, and prompt nitrogen oxides² at coal combustion [50, 81]. The analysis was made on the Kansk–Achinsk coal of the Irsha–Borodinsk deposit. The conventional chemical formula for the organic mass of this coal has the form: $\text{CH}_{0.833}\text{O}_{0.233}\text{N}_{0.012}\text{S}_{0.002}$. The greatest efforts were made to study dependences of the NO_x concentration on a) thermodynamic parameters, b) the composition of the reaction mixture, c) the process mechanism, and d) conditions of energy and mass exchange.

In the analysis the general MEIS was the basis for constructing models representing a real combustion process in sufficient detail and those employing utmost idealization of the mechanism of chemical reactions. The most detailed model comprised 200 components formed by 12 chemical elements. Coal's organic and mineral parts were presented. The vector x included 50 gaseous and condensed nitrogen compounds along with sulfur compounds, hydrocarbons, heavy metals, and other substances. Studies on reaction mixtures with such a wide composition of substances by kinetic modeling gives rise to many difficulties.

The results of calculation of equilibrium concentrations of nitrogen compounds (at the point x^{eq}) with the *air excess* coefficient³ $\alpha_{\text{air}} = 1.2$ obtained by the detailed model are presented in Fig. 5.5. Nitrogen monoxide (NO) prevails among these compounds, which agrees with experimental data. Figure 5.6 illustrates

² Thermal oxides are formed at fuel burning from atmospheric nitrogen and oxygen. Fuel oxides are the result of oxidation of nitrogen-containing compounds of coal. Prompt oxides are formed from atmospheric nitrogen as a result of its interaction with active species emerging at thermal destruction of the organic part of fuel.

³ The ratio between the available air and the stoichiometrically needed amount of it.

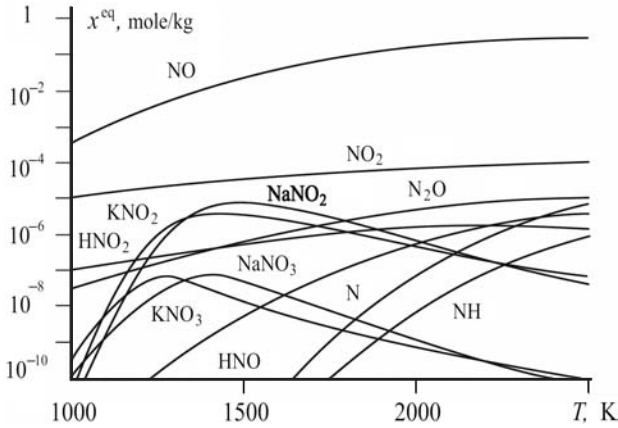


FIGURE 5.5. Equilibrium concentrations of nitrogen compounds in the products of the Kansk–Achinsk coal combustion ($\alpha_{\text{air}} = 1.2$).

dependences $x_{\text{NO}} = f(T)$ and $x_{\text{NO}} = \varphi(\alpha_{\text{air}})$. The figure shows a strong effect of temperature on the NO concentration and a sharp change of NO amount at the instant when the value of α_{air} exceeds unity (i.e., at a transition from the reductive to the oxidative medium). Figure 5.7 illustrates the interrelation between concentrations of NO and another dangerous pollutant—carbon monoxide (CO). The detailed model allowed the increasing yield of other incomplete combustion products to be determined at NO suppression; many of these are environmentally more hazardous than NO.

Now we will successively discuss the technique and the results of modeling the formation of thermal, fuel, and prompt NO_x .

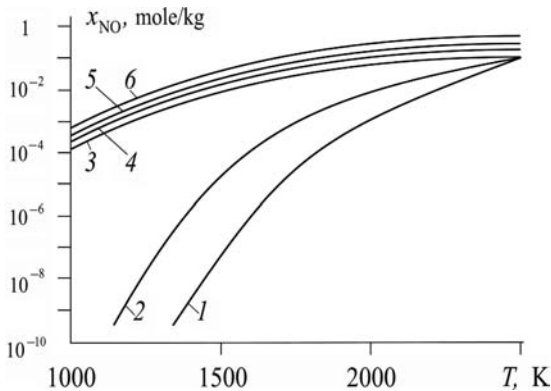


FIGURE 5.6. The equilibrium yield of NO versus combustion temperature and air excess α_{air} : 1, 0.95; 2, 1.00; 3, 1.05; 4, 1.10; 5, 1.20; 6, 1.40.

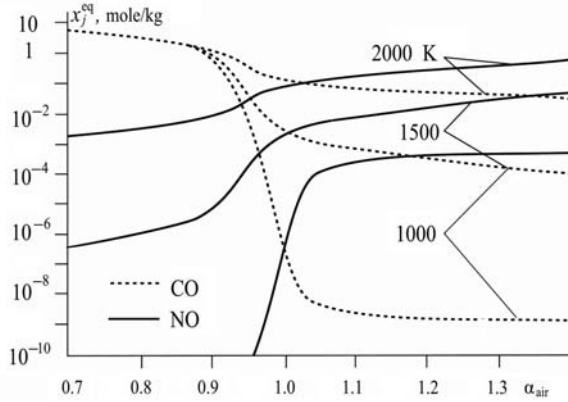
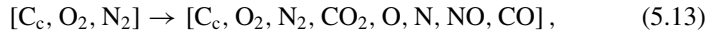


FIGURE 5.7. Equilibrium concentrations of NO and CO versus the air excess α_{air} at different combustion temperatures.

The fundamental laws in formation of thermal oxides were revealed with idealized models corresponding to the simplest systems of reagents:

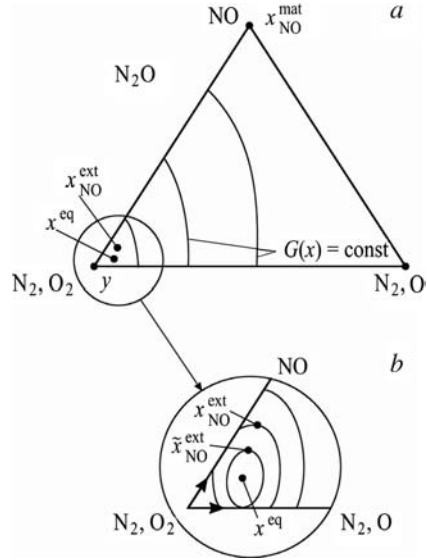


where the initial reagents (vector y) are given in the left-hand side brackets and the total compositions of the reaction mixture (vector x) are in the right-hand side brackets.

The simplest system (5.12) allows one to abstract from the reactions of fuel burning and study a pure process of molecular nitrogen oxidation at T and P typical of these reactions. System (5.13) reflects the key specific features of N_2 oxidation in the real coal-burning process. System (5.14) corresponds to Ya.B. Zeldovich's theory [173, 175] on the thermal nature of NO formation reactions at burning and explosion. According to this theory the difference in reaction rates causes formation of thermal oxides after the organic coal mass oxidation is completed. This system offers a better explanation of the available experimental data on the thermal NO_x formation than the two preceding ones.

The results of analysis for system (5.12) are illustrated in Fig. 5.8a and b. It presents the face $\text{N}_2, \text{O}_2(y) - \text{NO} - \text{N}_2, \text{O}$ of the material balance polyhedron $D(y)$ (Fig. 5.8a) and its small part adjacent to vertex y (Fig. 5.8b). The vertex NO corresponds to the state $x_{\text{NO}}^{\text{mat}}$. From Fig. 5.8b it is seen that thermodynamics assumes a concentration of $x_{\text{NO}}^{\text{ext}}$ that is somewhat higher than the equilibrium $x_{\text{NO}}^{\text{eq}}$. The extent of the excess depends on equilibrium location. The highest value of x_{NO} is reached when moving along $y - \text{NO}$ to the point with a minimum value of $G(x)$ at this edge (the thermodynamic "pothole") and then along the curve $G(x) = \text{const}$. The calculations have shown that superequilibrium concentrations of NO can take

FIGURE 5.8. To the thermodynamic analysis of NO formation in the system $[\text{O}_2, \text{N}_2, \text{O}, \text{NO}]$ $T = 2000 \text{ K}$, $P = 0.1 \text{ MPa}$.



place only starting with $T = 1600 \text{ K}$ and the difference $(x^{\text{ext}}_{\text{NO}} - x^{\text{eq}}_{\text{NO}})$ increases with the temperature rise. However, even at $T = 2000 \text{ K}$ this concentration still remains rather low (about 28%, Table 5.4). The thermodynamic attainability region $D_t(y)$ for system (5.12) is extremely small. The system enthalpies at the states x^{eq} and x^{ext} are approximately the same. But the inequalities $H(x^{\text{ext}}) > H(x^{\text{eq}}) > H(y)$ are observed, i.e., for the process to be realized a small energy inflow is required from the outside.

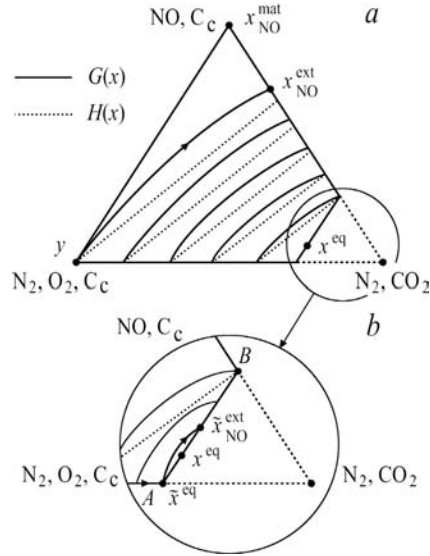
Specific features of systems (5.13) and (5.14) are explained from Fig. 5.9a and b. In (5.13) in comparison with (5.12) the thermodynamic attainability region (the nonhatched part of the triangle $y - x^{\text{mat}}_{\text{NO}} - \text{CO}_2, \text{N}_2$ in Fig. 5.9a) sharply increases, resulting in a considerable rise of the value of $x^{\text{ext}}_{\text{NO}}$ (Table 5.4). At $T = 1000 \text{ K}$ the point $x^{\text{ext}}_{\text{NO}}$ lies on the intersection of the curve $G = G(y)$ with the edge $x^{\text{mat}}_{\text{NO}} - \text{CO}_2, \text{N}_2$. At $T > 1000 \text{ K}$ the thermodynamic “pothole” occurs. The point $x^{\text{ext}}_{\text{NO}}$ has a very high enthalpy level $H(x^{\text{ext}}) \gg H(y)$. Hence, this point can be reached by the additional supply of a large amount of energy (520–970 kJ/kg at $T = 1000 - 3000 \text{ K}$) to the reaction mixture. In boiler furnaces such conditions are possible only in local zones, e.g., in the torch core.

In system (5.14) the point $y \approx \tilde{x}^{\text{eq}}$ is the initial point (Fig. 5.9b). It corresponds to equilibrium state (5.13), provided NO starts to form only after completion of carbon burning. The segment $[y, \tilde{x}^{\text{eq}}]$ in this case represents oxidation of C_c . The point x^{eq} corresponds to the final equilibrium of system (5.13), where there are no constraints on the process mechanism. When we pass to system (5.14), the thermodynamically attainable region (where a superequilibrium concentration of NO is possible) decreases considerably. In Fig. 5.9b the region is limited by the curve $G = G(\tilde{x}^{\text{eq}})$ and the straight line AB . The maximum NO concentration

TABLE 5.4. Formation of thermal nitrogen monoxide (NO) ($T = 0.1$ MPa)

T, K	x, mole/kg						$H(x) - H(y), \text{kJ/kg}$						$G(x) - G(y), \text{kJ/kg}$						$S(x) - S(y), \text{kJ/(kg}\cdot\text{K)}$						
	eq		ext		mat		eq		ext		mat		eq		ext		mat		eq		ext		mat		
System (5.12)																									
1000	0.0011	0.0011	14.56	0.1	0.1	1331	0	0	0	0	1099	0.0001	0.0001	0.0001	0.0001	0.0001	0.0001	0.0001	0.0001	0.0001	0.0001	0.0001	0.2328	0.2328	0.2328
1250	0.0098	0.0098	14.56	1.0	1.0	1332	-0.10	-0.10	-0.10	-0.10	1040	0.0009	0.0009	0.0009	0.0009	0.0009	0.0009	0.0009	0.0009	0.0009	0.0009	0.0009	0.2334	0.2334	0.2334
1500	0.0424	0.0424	14.56	4.0	4.0	1332	-0.50	-0.50	-0.50	-0.50	982	0.0030	0.0030	0.0030	0.0030	0.0030	0.0030	0.0030	0.0030	0.0030	0.0030	0.0030	0.2333	0.2333	0.2333
1750	0.1206	0.1377	14.56	11	13	1332	-1.80	-1.80	-1.80	-1.80	924	0.0073	0.0073	0.0073	0.0073	0.0073	0.0073	0.0073	0.0073	0.0073	0.0073	0.0073	0.2333	0.2333	0.2333
2000	0.2629	0.3399	14.56	27	34	1331	-4.60	-4.60	-4.60	-4.60	866	0.0158	0.0158	0.0158	0.0158	0.0158	0.0158	0.0158	0.0158	0.0158	0.0158	0.0158	0.2327	0.2327	0.2327
2250	0.4787	0.7278	14.56	59	81	1330	-10.10	-10.10	-10.10	-10.10	807	0.0307	0.0307	0.0307	0.0307	0.0307	0.0307	0.0307	0.0307	0.0307	0.0307	0.0307	0.2323	0.2323	0.2323
2500	0.7652	1.4020	14.56	127	184	1329	-20.90	-20.90	-20.90	-20.90	750	0.0592	0.0592	0.0592	0.0592	0.0592	0.0592	0.0592	0.0592	0.0592	0.0592	0.0592	0.2318	0.2318	0.2318
2750	1.1030	2.4680	14.56	270	385	1326	-41.70	-41.70	-41.70	-41.70	692	0.1133	0.1133	0.1133	0.1133	0.1133	0.1133	0.1133	0.1133	0.1133	0.1133	0.1133	0.2307	0.2307	0.2307
3000	1.4530	3.9750	14.56	544	729	1323	-81.00	-81.00	-81.00	-81.00	634	0.2083	0.2083	0.2083	0.2083	0.2083	0.2083	0.2083	0.2083	0.2083	0.2083	0.2083	0.2296	0.2296	0.2296
System (5.13)																									
1000	0.0004	0.0118	13.6	-2236	520	1243	-2268.6	0	0	1027	0.0329	0.0329	0.0329	0.0329	0.0329	0.0329	0.0329	0.0329	0.0329	0.0329	0.0329	0.0329	0.2168	0.2168	0.2168
1250	0.0037	0.061	13.6	-2238	631	1244	-2276.5	-0.1	-0.1	927	0.0308	0.0308	0.0308	0.0308	0.0308	0.0308	0.0308	0.0308	0.0308	0.0308	0.0308	0.0308	0.2175	0.2175	0.2175
1500	0.0161	0.1099	13.6	-2240	704	1244	-2283.9	-0.5	-0.5	918	0.0294	0.0294	0.0294	0.0294	0.0294	0.0294	0.0294	0.0294	0.0294	0.0294	0.0294	0.0294	0.2175	0.2175	0.2175
1750	0.0457	0.1131	13.6	-2239	765	1244	-2291.2	-1.7	-1.7	863	0.0297	0.0297	0.0297	0.0297	0.0297	0.0297	0.0297	0.0297	0.0297	0.0297	0.0297	0.0297	0.2175	0.2175	0.2175
2000	0.0998	0.1158	13.6	-2227	819	1243	-2299.2	-4.1	-4.1	809	0.0362	0.0362	0.0362	0.0362	0.0362	0.0362	0.0362	0.0362	0.0362	0.0362	0.0362	0.0362	0.2170	0.2170	0.2170
2250	0.1875	0.1183	13.6	-2163	865	1242	-2311.2	-8.5	-8.5	755	0.0661	0.0661	0.0661	0.0661	0.0661	0.0661	0.0661	0.0661	0.0661	0.0661	0.0661	0.0661	0.2165	0.2165	0.2165
2500	0.3307	0.1203	13.6	-1964	906	1241	-2336.7	-15.2	-15.2	701	0.1491	0.1491	0.1491	0.1491	0.1491	0.1491	0.1491	0.1491	0.1491	0.1491	0.1491	0.1491	0.2161	0.2161	0.2161
2750	0.5492	0.1221	13.6	-1583	939	1239	-2391.0	-24.7	-24.7	647	0.2938	0.2938	0.2938	0.2938	0.2938	0.2938	0.2938	0.2938	0.2938	0.2938	0.2938	0.2938	0.2153	0.2153	0.2153
3000	0.8138	0.1237	13.6	-1062	967	1236	-2486.8	-37.3	-37.3	593	0.4749	0.4749	0.4749	0.4749	0.4749	0.4749	0.4749	0.4749	0.4749	0.4749	0.4749	0.4749	0.2143	0.2143	0.2143
System (5.14)																									
1000	0.0004	0.0011	13.6	0.0	0.0	3479	0	0	0	0	3295	0.0000	0.0000	0.0000	0.0000	0.0000	0.0000	0.0000	0.0000	0.0000	0.0000	0.0000	0.1839	0.1839	0.1839
1250	0.0037	0.0101	13.6	0.0	0.0	3482	-0.10	-0.10	-0.10	-0.10	3249	0.0001	0.0001	0.0001	0.0001	0.0001	0.0001	0.0001	0.0001	0.0001	0.0001	0.0001	0.1868	0.1868	0.1868
1500	0.0161	0.0440	13.6	1.5	4.1	3485	-0.20	-0.20	-0.20	-0.20	3202	0.0011	0.0011	0.0011	0.0011	0.0011	0.0011	0.0011	0.0011	0.0011	0.0011	0.0011	0.1892	0.1892	0.1892
1750	0.0457	0.1277	13.6	5.3	13	3489	-0.80	-0.80	-0.80	-0.80	3154	0.0035	0.0035	0.0035	0.0035	0.0035	0.0035	0.0035	0.0035	0.0035	0.0035	0.0035	0.1914	0.1914	0.1914
2000	0.0998	0.3080	13.6	21	41	3491	-2.40	-2.40	-2.40	-2.40	3106	0.0119	0.0119	0.0119	0.0119	0.0119	0.0119	0.0119	0.0119	0.0119	0.0119	0.0119	0.1927	0.1927	0.1927
2250	0.1875	0.7106	13.6	89	145	3494	-8.50	-8.50	-8.50	-8.50	3058	0.0434	0.0434	0.0434	0.0434	0.0434	0.0434	0.0434	0.0434	0.0434	0.0434	0.0434	0.1939	0.1939	0.1939
2500	0.3307	1.5830	13.6	292	454	3497	-28.6	-28.6	-28.6	-28.6	3009	0.1282	0.1282	0.1282	0.1282	0.1282	0.1282	0.1282	0.1282	0.1282	0.1282	0.1282	0.1952	0.1952	0.1952
2750	0.5492	3.1410	13.6	679	1042	3501	-77.9	-77.9	-77.9	-77.9	2960	0.2752	0.2752	0.2752	0.2752	0.2752	0.2752	0.2752	0.2752	0.2752	0.2752	0.2752	0.1967	0.1967	0.1967
3000	0.8138	5.2340	13.6	1207	1743	3505	-169.3	-169.3	-169.3	-169.3	2911	0.4588	0.4588	0.4588	0.4588	0.4588	0.4588	0.4588	0.4588	0.4588	0.4588	0.4588	0.1982	0.1982	0.1982

FIGURE 5.9. To the thermodynamic analysis of NO formation in the system $[C_c, O_2, N_2, NO, CO_2]$. $T = 1500$ K, $P = 0.1$ MPa.



(the point \tilde{x}_{NO}^{ext}) also decreases in a pronounced fashion. This outcome is typical primarily of low temperature burning ($T < 1500$ K).

The negative thermal effect of NO formation in system (5.14) increases sharply with rising temperature (Table 5.4). Constraints on energy and mass exchange are the main reason for discrepancy in the theoretical and experimental data on the NO yields at $T > 1500$ K.

Comparison of systems (5.13) and (5.14) results in the key conclusion that a new mechanism of NO formation (*Fenimore's mechanism*) originates at injection of condensed carbon into the reaction volume [48]. Nitrogen oxides formed by this mechanism are called “prompt.” Thus, in system (5.13) the value of x_{NO}^{ext} is the sum of thermal and prompt nitrogen oxides. In the whole region $D_i(y)$, except for its negligible part, limited by the curve $G = G(\tilde{x}^{eq})$ and the segment AB , the nitrogen monoxide is formed by the “prompt” mechanism.

Fig. 5.9b illustrates the second important conclusion of the analysis. In the case of kinetic slowdown of formation reactions, emissions of thermal NO lower than the equilibrium emissions are possible if the fuel is burnt completely. The corresponding states lie in the region limited by the lines AB and $G = G(\tilde{x}^{eq})$ below the point x^{eq} . At the point A the NO concentration is close to zero. With increasing combustion temperature, the point x^{eq} is displaced along AB toward B , i.e., toward the region of higher concentrations (Fig. 5.9b). The same regularity is observed with respect to the extreme states x_{NO}^{ext} and \tilde{x}^{eq} .

With the expansion of system (5.13) (increase of the vector x dimension to $n = 200$, which is quite enough to describe the oxidation of organic part of coal) the equilibrium and extreme concentrations of NO at $T < 2000$ K change negligibly.

Divergence does not exceed 4% for $x_{\text{NO}}^{\text{eq}}$ and 15% for $\bar{x}_{\text{NO}}^{\text{ext}}$ (in a real system the NO yields are lower). At $T > 2000$ K divergence increases, making at $T = 3000$ K 10% for $x_{\text{NO}}^{\text{eq}}$ and 60% for $\bar{x}_{\text{NO}}^{\text{ext}}$. As to differences in $x_{\text{NO}}^{\text{ext}}$, they do not exceed 10–20% over the whole studied range of temperatures. The experimental data on $x_{\text{NO}}^{\text{ext}}$ are somewhat higher.

The thermodynamic analysis performed contributes to substantiation of ways to lower the formation of thermal oxides (NO_x) during fuel combustion, namely: 1) decrease of combustion temperature ($T < 1500$ K); 2) decrease of the time for the flue gases to stay in the high temperature zone of the furnace; 3) decrease of α_{air} in the furnace (however, α_{air} should be higher than unity at its outlet); 4) limitation of energy liberation in the high-temperature zone (by more intensive heat removal from it); 5) elimination of carbon injection into the high-temperature zone of the furnace.

According to the up-to-date concept [147, 165], fuel nitrogen oxides are obtained from nitrous substances of coal in the starting section of torch, when temperatures reaches 900–1000 K. During thermal destruction of nitrous substances of fuel the intermediate gaseous substances R_N —the molecules of HCN, NH_3 , and the radicals CN, NH, and NH_2 —are formed first. Then these products react with the atmospheric oxygen and the flame components O and OH with partial oxidation to NO. In general, the fuel NO formation can be represented in the form:



where Q is thermal energy.

The calculations show that, in terms of thermodynamics, between the temperatures 600–1000 K, the fuel nitrogen may virtually completely turn into the gaseous nitrogen species HCN, CN, NH_3 , etc.; i.e., process (5.15) has no thermodynamic constraints. Hence, the condition $x_j^{\text{ext}} = x_j^{\text{mat}}$ is met for all R_N . In Fig. 5.10 this conclusion is illustrated on the example of NH_3 .

The maximum (thermodynamically permitted) total concentration of the nitrogen compounds in products of thermal destruction of coal is about 0.24 mole N/kg.

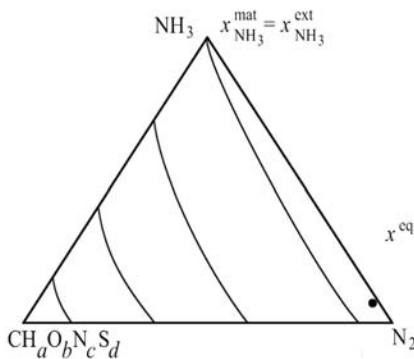
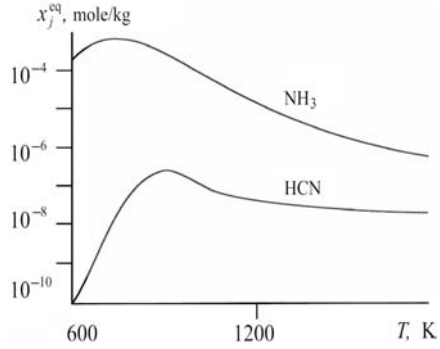


FIGURE 5.10. To the thermodynamic analysis of thermal destruction of nitrogen species of coal ($\alpha_{\text{air}} = 0.8$; $P = 0.1$ MPa, $T = 1000$ K).

FIGURE 5.11. The equilibrium concentrations of gaseous nitrogen substances in the products of thermal coal destruction ($\alpha_{\text{air}} = 0.8$; $P = 0.1$ MPa).



The concentration does not depend on T and α_{air} : it is determined entirely by the content of the bound nitrogen in fuel. It should be noted here that the point x^{eq} is closely “held” against the edge $\text{NH}_3 - \text{N}_2$ inside $D(y)$.

After the complete equilibrium is reached, the concentrations of R_N sharply fall (by 3–5 orders of magnitude and more) and do not exceed $5 \cdot 10^{-4}$ mole/kg at $\alpha_{\text{air}} = 0.8$. Among the considered substances in the equilibrium mixture, NH_3 and HCN are present in the greatest amounts. Their equilibrium concentrations depend on T and particularly on α_{air} . At $T < 1000$ K the concentrations of HCN fall rapidly, while those of NH_3 on the contrary remain constant and are the highest (Fig. 5.11). The influence of air excess is more unambiguous. The increase in α_{air} leads to a decrease in the yields of NH_3 and HCN , and at $\alpha_{\text{air}} > 1$ the concentrations of these substances are virtually equal to zero (Fig. 5.12).

The thermodynamic analysis of R_N oxidation into NO (5.16) reveals that thermodynamic constraints are also inessential for this process. Hence $x_{\text{NO}}^{\text{ext}} = x_{\text{NO}}^{\text{mat}}$ (Fig. 5.13). The material balance constraints on oxygen are more significant (the segment AB in Fig. 5.13). When the oxygen content in the system decreases, the line AB shifts downward, and, correspondingly, the values of $x_{\text{NO}}^{\text{ext}}$ decrease. Note that in this case the solution is degenerate. At any point of the segment AB , $x = x_{\text{NO}}^{\text{ext}}$. The extreme NO yield does not depend on temperature in the range from 600 to 2400 K.

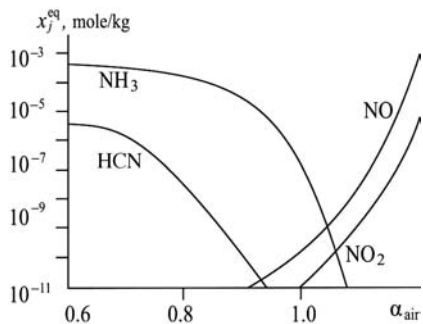


FIGURE 5.12. Dependence of equilibrium concentrations of nitrogen species R_N in the products of thermal coal destruction on α_{air} ($T = 1000$ K; $P = 0.1$ MPa).

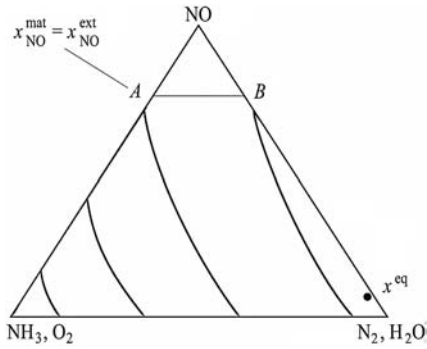


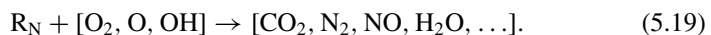
FIGURE 5.13. To the thermal analysis of fuel NO formation.

At the state x^{eq} of the process (5.16) the NO concentration is by several orders of magnitude lower than it is in $x_{\text{NO}}^{\text{ext}}$. Here, the equilibrium concentrations of NO depend strongly enough on T , especially in the region $T < 1000$ K. They show weaker dependence on α_{air} (at $\alpha_{\text{air}} > 1$), increasing with its rise. This dependence is inverse to that in the process (5.15), where the R_{N} yield decreases with the rising α_{air} (Fig. 5.12).

Results of the thermodynamic analysis of the processes (5.15) and (5.16) allow the conclusion that the yield of fuel NO_x depends rather weakly on T and very strongly on oxygen content in the combustion zone. This is in a good agreement with experimental data [165].

From the aforesaid follow some recommendations on reduction of fuel NO_x formation: 1) change in the composition of primary products of thermal decomposition of nitrogen species to enhance the extent of fuel nitrogen transition to molecular nitrogen (in particular, by more intensive elimination of volatiles, their thorough premixing with air, and creation of an oxidizing medium in the heating zone of coal particles); 2) more extended period for thermal destruction products to stay in the torch volume to achieve more complete reactions of R_{N} transition to N_2 and NO reduction (to the point of complete equilibrium state); 3) decrease of the oxidizer content in the combustion zone until the reducing atmosphere is created in it; 4) use of fuel without bound nitrogen.

According to C.P. Fenimore [48], prompt nitrogen oxides are formed at the flame front from atmospheric nitrogen by the following mechanism: As a result of the thermal destruction of organic coal matter, the carbon substances R_{C} (CH , CH_2 , C) are formed first. They are bound with molecular nitrogen, forming substances such as R_{N} (HCN , CN , NH , N , etc.). The latter react with the active species of flame O , H , and OH , resulting in formation of the prompt oxides. The overall process can be represented in the form



The MEIS-based studies revealed the possibility for forming O, H, and OH in the flame at coal burning in amounts that exceed their equilibrium concentrations by several orders of magnitude. This is, however, a very energy-capacious process. Without constraints on energy supply to the reacting system the limiting (thermodynamically allowed) concentrations of O, H, and OH in the products of coal combustion in the temperature range 600–1200 K vary as follows (at $\alpha_{\text{air}} = 1.2$): The volumetric fractions of O and H increase linearly from 5.8 and 10.2% to 10.8 and 16.1%, respectively, and the OH fraction decreases linearly from 10.8 to 5.2%. Energy consumption for formation of such quantities of O, H, and OH and the corresponding changes in the composition of the whole reacting system within the same temperature range (600–1200 K) linearly increase from 660 to 1650 kJ/kg. It is usually impossible to supply such quantities of energy in real furnaces. The yield of active species sharply falls with decrease of heat supplied. For the equilibrium state at low T it is close to zero. In a boiler, sources of additional energy may comprise: a) radiation from the high-temperature flame zone, b) hot recirculating gases, and c) exothermal chemical reactions running directly in this zone.

Thermodynamic constraints on the formation of extreme concentrations of O, H, and OH are significant. The points x^{ext} lie on the curve $G = G(y)$. The temperature rise causes extension of the thermodynamic attainability region $D_t(y)$. The equilibrium concentrations of O, H, and OH are in strong dependence on T and α_{air} (Fig. 5.14). All of them intensively increase at the increase of T . Increase of α_{air} leads to yield increases of O and OH and yield decrease of H.

We carried out a study on thermodynamic regularities in the formation of R_C radicals at the thermal destruction of organic coal mass by scheme (5.17). The point x^{ext} is located on the initial surface of the Gibbs energy $G(y)$ (Fig. 5.15). It can be reached by the considerable quantity of energy supplied from the outside. The value of $x_{\text{CH}}^{\text{ext}}$ smoothly increases with rise in temperature.

At $\alpha_{\text{air}} > 1$ the equilibrium concentrations of R_C are negligible within the considered temperature range 750–2000 K. The point x^{eq} in this case lies near the vertex CO_2 of the polyhedron $D(y)$.

The thermodynamic analysis of process (5.18) lets us conclude the following: There are no thermodynamic constraints for this process, therefore, the states

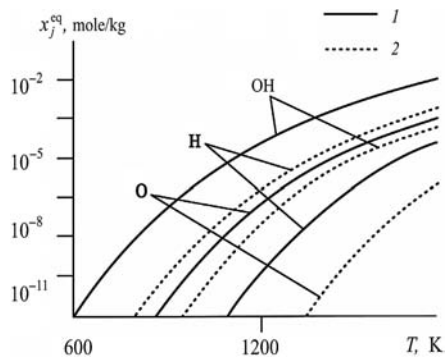


FIGURE 5.14. Equilibrium concentrations of O, H, OH in the flame at coal burning $\alpha_{\text{air}} : 1, 1.2; 2, 0.8$.

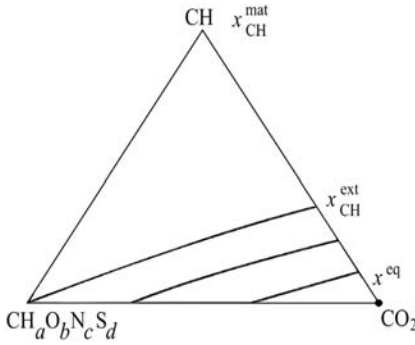


FIGURE 5.15. Thermodynamics of CH radical formation at thermal destruction of coal: $T = 1000$ K; $P = 0.1$ MPa; $\alpha_{\text{air}} = 1.2$; y , mole: $y_{\text{OCM}} = 1$, $y_{\text{O}_2} = 1.312$; x , mole/kg: $x_{\text{CH}}^{\text{eq}} = 0$, $x_{\text{CH}}^{\text{ext}} = 9.02$, $x_{\text{CH}}^{\text{mat}} = 14.18$; $G(x)$, kJ/kg: $G(y) = -4695$, $G(x^{\text{eq}}) = -13160$, $G(x_{\text{CH}}^{\text{ext}}) = -4695$, $G(x_{\text{CH}}^{\text{mat}}) = 1125$.

$x_j^{\text{ext}} = x_j^{\text{mat}}$ are attainable for all compounds of the R_N type. The extreme concentrations of R_N depend neither on α_{air} nor T and are wholly determined by the concentrations of R_C radicals in the system. The equilibrium concentrations of R_N are by several orders of magnitude lower than the extreme ones. Comparatively speaking, they relatively weakly depend on temperature and strongly on α_{air} in the range $0.8 < \alpha_{\text{air}} < 1.2$. At $\alpha_{\text{air}} < 0.8$ the equilibrium concentrations of R_N stabilize and make up approximately 10 mole/kg; there is a prevalence of NH_3 in these amounts. The concentrations of R_N rapidly decrease with increasing α and with $\alpha > 1$ do not exceed 10^{-9} mole/kg.

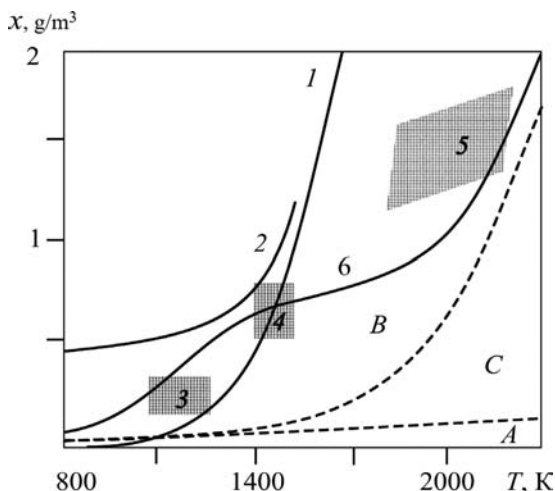
The regularities in formation of prompt nitrogen oxides by scheme (5.19) are similar to those in the oxidation of the products of thermal coal destruction into fuel nitrogen oxides represented in process (5.16).

Small changes in the yield of carbon radicals CH and the total concentration of active species O, H, and OH at the flame front within the wide temperature range explain the weak dependence of the yield of prompt NO on temperature, a conclusion that agrees with experimental data [157].

The analysis of specific features in the formation of prompt NO_x determines potential measures for eliminating this situation: 1) operation of the process of thermal coal destruction at the low temperature and $\alpha_{\text{air}} > 1$ (to decrease the yield of carbon radicals); 2) implementation of “cold” flame regime in the reductive medium (which will contribute to decrease in concentrations of O, H, and OH); 3) limited supply of high-temperature energy to the zone of thermal destruction of coal organics and to the flame front from the outside (to reduce the yield of CH, O, H, and OH); 4) prevention of the reactions of atmospheric nitrogen-binding by the carbon radicals (by creating an oxidative medium in the corresponding furnace zone); 5) change in the mechanism of fuel burning to decrease concentrations of O, OH, H, R_C , and R_N in the reacting volume (e.g., implementation of low-temperature catalytic oxidation); 6) application of pure oxygen rather than air as an oxidizer; 7) changeover to carbon-free fuel combustion (e.g., hydrogen produced from coal).

The thermodynamic analysis of mechanisms for forming individual types of nitrogen oxides reveals the following general approaches to reduction of the

FIGURE 5.16. Comparison of the theoretical and experimental yields of NO at coal combustion: equilibrium (1), extreme (maximum) (2); actual data (3–6): fluidized-bed combustion (3); low-temperature burning of brown coals (4); high-temperature burning of hard coals (5); average NO emissions by pulverized coal-fired boilers (6); A: “prompt” NO_x; B: “fuel” NO_x; C: “thermal” NO_x.



thermodynamic feasibility region of NO_x formation reactions:

1. Limitation of energy supply to the zones of intensive formation of NO and R_C.
2. Limitation of oxygen consumption by the reaction mixture at the initial combustion stage.
3. Increase in duration of combustion products presence in the reduction zone.
4. Decrease in the temperature level at the initial combustion stage (to minimize active flame components O, H, and OH).
5. Decrease in the temperature and the air excess coefficient in the torch center.

MEIS-based theoretical concentrations of NO (equilibrium, maximum, and minimum) were compared with generalized experimental data taken from [14, 68, 157] (Fig. 5.16). Joint analysis of sufficiently well-corresponding calculated and experimental data explains basic regulations of formation of nitrogen oxides and allows the conclusions on the possibility of applying thermodynamics to, potentially, improve fuel combustion technologies aimed at reduction of NO_x yield.

In the region of low combustion temperatures ($T < 1500$ K) total NO_x emissions consist basically of fuel and prompt NO. Thermal NO yields prevail at $T > 2000$ K. In the temperature range 1500–2000 K (the region of torch-furnace boiler operation) the greatest contribution is made by fuel and thermal NO.

At $T < 1500$ K the actual NO emissions by pulverized coal-fired boilers can considerably exceed equilibrium values. The reason is the superequilibrium formation of fuel and prompt NO in the boilers. At high-temperature fuel combustion the NO yield does not reach, as a rule, an equilibrium value because of insufficient duration of reaction mixture presence in the region of maximum temperatures.

However, not all theoretical methods mentioned to reduce NO_x yields are of practical importance (for example, by reason of increasing concentrations of other harmful substances) and some of them contradict one another. Choice of tradeoff

decisions for specific type of furnaces and kind of fuel involved is an engineering problem whose successful solution may demand additional experimental and kinetic studies. The aim of these studies is to search for and realize on the thermodynamically attainable set $D_t(y)$ a process trajectory leading to the desirable result. The theoretical results discussed above may form a basis for this search.

After describing the considered example's significance in the direct solution of the problem of NO_x suppression in fuel combustion processes, we will take advantage of a visualization of the example to demonstrate the "art of the possible" in the thermodynamic analysis of technical systems.

In the given case such an analysis was made based on solely the fragmentary kinetic information on the studied process mechanism: an aggregated description of forming three types of nitrogen oxides. In real systems these processes are interrelated and in addition to this, their implementation depends on the whole set of reactions running in the system.

The fragmentary character of information was taken into account by applying the following scheme of thermodynamic modeling: Idealized models of the least dimension were used to study independently every parallel branch of the total mechanism of NO_x formation. The study of an individual branch, in turn, was reduced to the thermodynamic analysis of components of its aggregate stages. The influence of nonideality was evaluated by detailed models including nitrogen oxides and many other harmful compounds.

It is precisely such a stage-by-stage joint application of thermodynamics and kinetics, ideal and detailed "real" models, that allowed the fundamental regularities of running the considered processes to be revealed and the potential changes in the actual characteristics to be evaluated. The most important applied result of the analysis performed was the substantiation of measures on control of separate stages.

In our opinion the conclusions drawn proved to be more informative than those reached by the use of only kinetic models and full-scale experiments with a comparable scope of studies. The original results of the analysis carried out that were obtained by its "thermodynamic decomposition" are: 1) explanation of the reasons for changing sizes of the thermodynamic attainability region $D_t(y)$ with indication of possible quantitative relationships between $x_{\text{NO}}^{\text{mat}}$, $x_{\text{NO}}^{\text{ext}}$, $x_{\text{NO}}^{\text{eq}}$; 2) determination of the effect of nonthermodynamic factors (energy and mass exchange, air surplus) on NO_x concentrations; 3) appraisal of the possibility to decrease NO_x yield below the equilibrium values in the case of complete combustion of fuel carbon; 4) thermodynamic derivation of a weak temperature dependence of prompt NO_x formation.

Analysis of Environmental Characteristics of Periodic Fuel Combustion in Small Furnaces

Coal- or wood-fired utility boiler plants and home heating stoves with manual fuel loading are chosen as the object of study. In many cities these small heat sources

make the greatest contribution to air pollution by carbon monoxide, nitrogen and sulfur oxides, particulates (ash) and other harmful emissions.

The theoretical, in particular thermodynamic, analysis of combustion processes in these heat sources is apparently even more sophisticated than the study of pulverized fuel combustion in large furnaces. The first difficulty is caused by the unsteady and periodic behavior of the combustion process, characterized by small (between fuel loadings) and long (between cleanings of the fire grate) cycles. Periodic poking of the fuel as it burns in the bed is an additional source of the unsteadiness.

Periodicity makes an essential contribution to increase in a reacting system's nonequilibrium, and to temperature difference that arises between newly loaded and burning fuel, between solid and gas phases in the bed, and between the bed and furnace space over it.

Unfortunately, the problems in modeling are aggravated by the low technological level of equipment at small heat sources, the poor quality of fuel used, and in many cases by the low level of their operation. Because of highly nonuniform coal particle size distribution and low-quality poking, the layer of burning fuel becomes spatially nonuniform, conditions of mass exchange between phases and, hence, conditions of fuel ignition and burning, sharply deteriorate. Correspondingly, difficulties arise when we try to represent such "abnormal" conditions in theoretical models.

In comparison to the analysis of processes in large boilers another problem in studying the periodic combustion in small fixed-bed furnaces arises from the obvious insufficiency of theoretical and experimental data on the kinetics of the formation of harmful substances during such burning.

The mentioned specific features of the given example lead to distinctions in its thermodynamic analysis as compared to the previous example. Whereas, in the considered case of stationary burning, thermodynamics was used jointly with kinetics, the study presented below incorporates three interrelated elements: thermodynamics, kinetics and full-scale experiments. Surely, the experimental data are applied in virtually in all cases of thermodynamic modeling of complex real systems. However, here a full-scale experiment is directly included in the scheme of analysis.

MEIS application to periodic nonequilibrium combustion processes studies was based on an assumption about low variation of the macroscopic parameters in every local furnace (bed) volume—sufficiently low that it was possible to consider the processes running in the furnace as passing through the continuous sequence of equilibrium states.

The process mechanism was broken down into three aggregate stages [138]. Two of them ("come-out" and combustion of volatiles, and combustion of residual coke) refer to the bed; the third represents chemical transformations in the furnace space.

The first two stages were analyzed on the basis of a joint application of thermodynamics and full-scale experiments. Kinetic modeling was unnecessary because of the rather fast processes of coal thermal destruction. Such modeling would also be rather difficult because of the highly sophisticated kinetic description of

a heterogeneous coal burning. Experiments resulted in determination of: 1) temperature variations in the bed as a function of time and average temperature for individual stages of the total process; 2) time dependences of α_{air} and variations of this magnitude on the bed surface; and 3) concentrations of individual substances (O_2 , CO , CO_2 , etc.) at the bed boundary. The experimental data helped prepare correctly a list of the vector x components and specify the temperature of the reaction mixture by the MEIS-based variant calculations.

We carried out analysis of the third stage (the processes in the furnace space above the bed) by using all three mentioned elements of the applied technique: thermodynamic, kinetic, and full-scale experimentation. Kinetic calculations were applied to determine concentrations of substances (e.g., NO_x), whose formation time can presumably exceed the time during which the gas flow passes through the furnace space. Since there are no reliable data on the mechanism and constants of chemical reaction rates with participation of aromatic hydrocarbons, in particular polycyclic aromatics (PAH), their formation was determined by MEIS. As in the analysis of the first two stages, the experimental data on the time-dependence of T , α_{air} , and concentrations of particular substances (e.g., CO) at the furnace outlet were also applied to the MEIS-based variant calculations.

Some results of the analysis on the estimation of concentrations of harmful substances formed at combustion are presented in Figs. 5.17, 5.18, 5.19, and 5.20.

Formation of nitrous substances (Fig. 5.17) was studied in accordance with the real course of reactions in time. As a result of the fixed-bed combustion almost all fuel nitrogen passes to molecular N_2 , which is favored by reductive conditions in the bed. Thermal NO_x yields make up only a small fraction of the total yield of NO_x . In the thermodynamic calculations the volatile nitrous substances were modeled by ammonia (NH_3) and prussic acid (HCN). The region of intensive formation of NH_3 and HCN (sources of fuel NO) corresponds to low temperatures and small α_{air} (Fig. 5.17*a* and *b*). The intermediate compounds are converted to fuel NO owing to high temperatures and higher air excess (Fig. 5.17*c*). Such conditions are observed in the bed during come-out and burning of volatile substances. The highest NO concentrations in the flue gases are noted precisely during burning of volatiles, which was confirmed by the authors' experiments.

Analysis of the composition of sulfur-containing compounds revealed that hydrogen sulfide (H_2S) and carbonyl sulfide (COS) can be formed along with SO_2 at fixed-bed combustion (Fig. 5.18). With the lack of oxidizer they can be formed in a rather wide temperature range, which causes a danger from high-temperature corrosion of the radiation heating surfaces.

The analysis also allowed us to determine conditions for formation of carbon monoxide CO , a most dangerous product of fuel combustion in the fixed bed at the stage of residual coke combustion (Fig. 5.19).

The results of analysis of changes in the PAH concentrations during combustion proved to be interesting. The experiments carried out by the authors jointly with A.G. Gorshkov and L.I. Belykh revealed that the PAH concentrations, which are products of incomplete combustion, depend to a greater extent not on the properties of fuel burnt, but on process conditions (Fig. 5.20). According to experimental

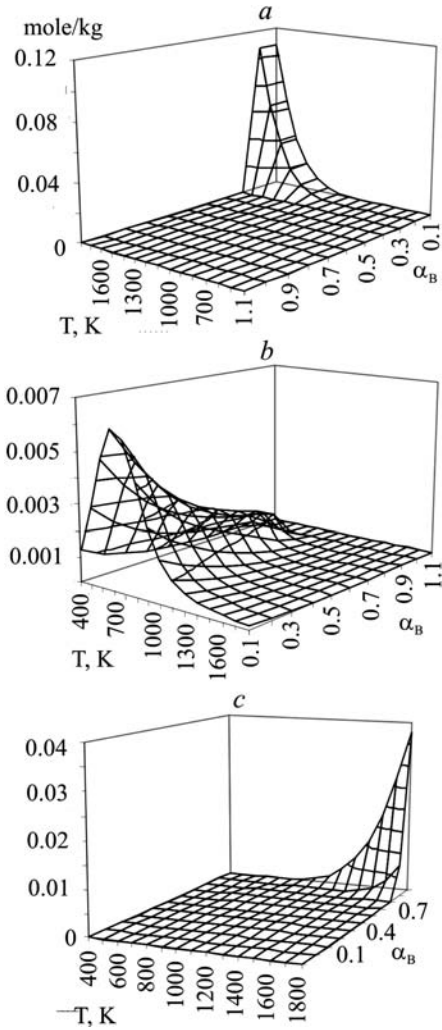


FIGURE 5.17. Equilibrium concentrations of nitrous products versus temperature and oxidizer excess. *a*) HCN, *b*) NH_3 , *c*) NO.

data, during the combustion cycle the PAH amount changes in a way similar to the way that concentration of particulates is effected. Therefore, it can be supposed that aromatic polycyclic hydrocarbons precipitate on solid particles. This relation is particularly clear at the initial stage of the combustion cycle, where, by the data of element analysis, soot constitutes 65–70% of the mass of solid particles. Thermodynamic calculations confirmed the supposition that PAH presence in coal combustion products was more likely the result of PAH synthesis at the gas phase oxidation of volatiles than the consequence of incomplete destruction of the carbon matrix of fuel.

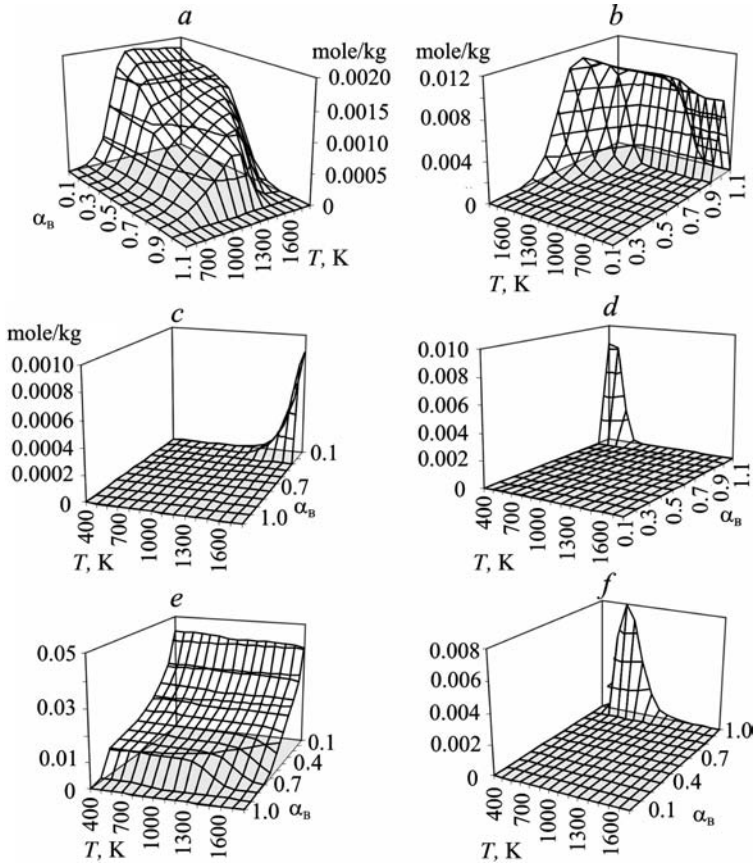


FIGURE 5.18. Equilibrium concentrations of sulfur-containing products versus temperature and oxidizer excess. a) – COS, b) SO₂, c) CS₂, d) H₂ SO₄, e) H₂ S, f) SO₃.

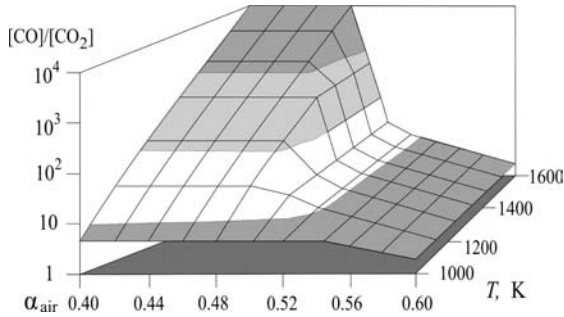


FIGURE 5.19. Dependence of the ratio $[CO]/[CO_2]$ on the air excess and temperature (thermodynamic equilibrium).

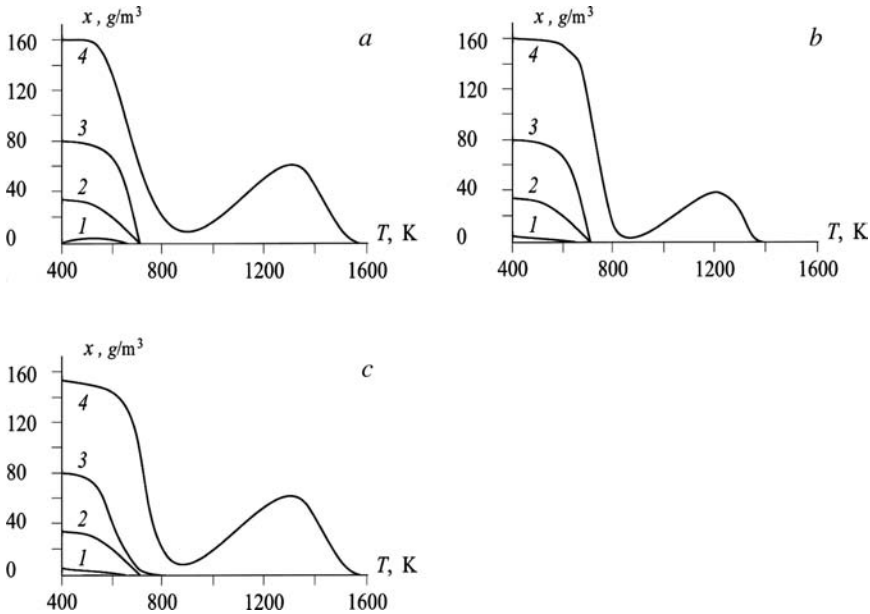


FIGURE 5.20. Equilibrium PAH concentrations versus combustion temperature at different air excesses. *a*) $\text{C}_{14}\text{H}_{10}$, anthracene gas; *b*) $\text{C}_{14}\text{H}_{10}$:*c*, condensed anthracene; *c*) $\text{C}_{14}\text{H}_{10}$, phenanthrene gas. α_{air} : 1, 0.4; 2, 0.3; 3, 0.2; 4, 0.1.

In modeling coal pyrolysis none of PAH is found in the state x^{eq} , when we include the condensed carbon C_c into vector x . In modeling transformations of volatiles, when we exclude C_c from the vector x , a number of PAH are found in the reaction mixture both in gaseous and in condensed phases at low α_{air} . The nature of change in calculated PAH concentrations versus temperature proved to be close to experimental data. The revealed relationships confirmed that the greatest amount of PAH is formed at the initial stage of combustion at lower temperatures and air excesses.

On the whole, the analysis of periodic fuel burning in fixed-bed furnaces enabled us to obtain sufficiently full information on the conditions for formation of harmful substances at different process stages and to determine environmentally optimal conditions of its implementation.

It was established that the real temperatures and air-excess coefficient in the bed at the initial combustion stage correspond to conditions of the low-temperature oxidation pyrolysis of solid fuel that leads to formation of products of incomplete combustion: carbon monoxide, soot, PAH, etc. Despite the high values of α_{air} in the furnace volume, the products of incomplete combustion formed due to low temperature and their short residence in the boiler do not have reasonable time for further oxidation; they are emitted to the atmosphere with flue gases. The quantity of these products can be reduced by feeding fuel in small portions and maintaining the temperature at a level sufficient for its fast ignition in the combustion zone.

Increase in average (for the cycle) furnace temperature causes some increase in thermal NO_x emissions. However, the thermodynamic calculations showed that this increase is negligible, since even at the maximum temperatures (1500–1600 K) in the fixed-bed furnaces the yield of thermal oxides is only a small portion of the total NO_x . High-temperature fuel pyrolysis at the initial stage of the combustion cycle fosters a decrease in concentrations of fuel nitrogen oxides owing to reduction of nitrogen substances to molecular nitrogen. The level of reduction is determined by the time, as nitrogen substances are found in the high-temperature zone.

Change in fuel combustion conditions virtually has no influence on SO_2 emission mass, since the atmosphere in the furnace space is oxidative. Increase in combustion temperature, however, makes it possible to prevent high-temperature corrosion of the furnace heating surfaces by sulfur oxides. A sufficiently high temperature maintained in the bed and the furnace space of boilers and stoves during the whole combustion period leads to a decrease in emissions of harmful substances (except for nitrogen and sulfur oxides) at all process stages.

Thermodynamic analysis of periodic fuel combustion processes in fixed-bed furnaces is undoubtedly useful to the task of recommending (in general) choice of heat supply schemes for residential districts, types of heat sources, kinds of fuel consumed, and so on.

5.3. Fuel Processing

We present some more examples on MEIS application to fossil fuel processing in order to form something close to a comprehensive notion of the capabilities of thermodynamic equilibria models.

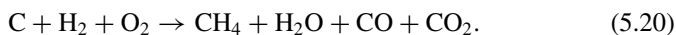
The authors have already used MEIS extensively for the analysis of basic technologies of deep coal conversion: hydrogenation and hydrogasification, pyrolysis, successive gasification and synthesis of liquid and gaseous hydrocarbons and methanol from the mixture of CO and H_2 , and hydrogen production to determine the limits of their perfection [81]. As in the study of combustion processes, Kansk–Achinsk coal was taken as the main object of study.

Here we present a brief thermodynamic analysis of two processes of methane production from coal: one by hydrogasification and steam conversion and the other by plasma gasification.

Hydrogasification of Coal

The first example, and the examples that follow, were analyzed on the simplest of models, ones in which coal was represented by condensed carbon, and the vector x included only key macrocomponents of the reaction mixture.

In a generalized form the hydrogasification process can be presented as follows:



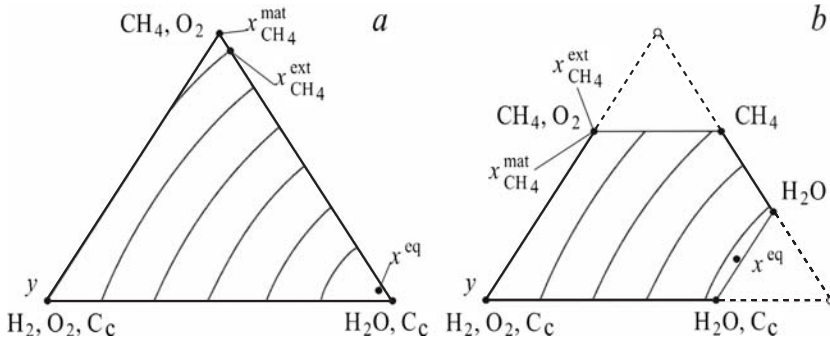


FIGURE 5.21. Geometrical interpretation of coal hydrogasification process. $P = 10$ MPa, $T = 800$ K; initial composition, mole: a) y : 1 C_c , 2 H_2 , 1 O_2 ; b) y : 1 C_c , 3 H_2 , 1 O_2 .

Fig. 5.21 represents graphically this process for the case when only CH_4 and H_2O are the reaction products.

When oxygen is consumed in large amounts, the final equilibrium point x^{eq} lies immediately adjacent to the vertex H_2O . The equilibrium yield of CH_4 is close to zero. When the system passes from vertex C_c , H_2 , O_2 (y) to vertex CH_4 , O_2 (corresponding to the maximum concentration of methane on $D(y) - x_{CH_4}^{mat}$, a thermodynamic “pothole” occurs. Therefore, the condition

$$x_{CH_4}^{ext} < x_{CH_4}^{mat}$$

is met (Fig. 5.21a).

At certain ratios of H:C, H:O and C:O there appear material balance constraints on carbon (the segment $[CH_4, O_2 - CH_4]$ in Fig. 5.21b) and oxygen (the segment $[H_2O, C - H_2O]$). Conditions when these constraints appear can be determined based on the technological ratios for the reaction synthesis of substances from the initial elements:

- at $H:C > 4$ we have a carbon constraint;
- at $H:O > 2$ we have an oxygen constraint (assuming that O_2 completely converts to H_2O);
- at $C:O > 0.5$ we also have an oxygen constraint (on the assumption that O_2 completely converts to CO_2). The latter constraint takes place when CO_2 is included in the list of reaction products instead of H_2O .

With the carbon constraint, the solution $x_{CH_4}^{ext}$ proves to be degenerate and can be situated at any point of the segment $[CH_4, O_2 - CH_4]$ belonging to the thermodynamic attainability region $D_t(y)$ (Fig. 5.21b). This means an increasing degree of freedom in the choice of chemical process trajectories in the space of compositions that provide the same maximum yield of methane.

With the more strict constraint on oxygen, the segment $[H_2O, C - H_2O]$ moves toward the edge $[y - CH_4, O_2]$ (Fig. 5.21b). The region accessible for the hydrogasification process decreases. The final equilibrium point x^{eq} shifts, approaching the

vertex CH_4 , C_2 and the edge $[y - \text{CH}_4, \text{O}_2]$. In the limit, when O_2 is not consumed, the point x^{eq} lies at this edge and the equilibrium detour becomes impossible.

If the oxygen is excluded from the vector y in system (5.20), at $T < 900 \text{ K}$ and $P > 1 \text{ MPa}$, the point x^{eq} closely approaches the vertex CH_4 . In this case, if we assume a small error, we can consider that

$$x_{\text{CH}_4}^{\text{eq}} = x_{\text{CH}_4}^{\text{ext}} = x_{\text{CH}_4}^{\text{mat}}.$$

At $T > 900 \text{ K}$ and $P > 1 \text{ MPa}$ the equilibrium yield of CH_4 begins to decrease and the point x^{eq} shifts to the vertex y .

With the growing dimensionality of the vector x (in particular, with inclusion of CO_2 in it), the thermodynamic constraints are removed and, in the studied temperature range 400–1200 K, the extreme yields of CH_4 depend only on the material balance constraints, i.e.,

$$x_{\text{CH}_4}^{\text{ext}} = x_{\text{CH}_4}^{\text{mat}}.$$

However, the equilibrium concentrations of CH_4 herewith decrease with the growing amount of oxygen in the system. This conclusion also holds for the case of coal hydrogasification by pure hydrogen, when coal is the oxygen source.

The presented analysis can obviously be useful when choosing conditions for the processes in real gasifiers.

Steam Coal Conversion

The generalized equation of this process is

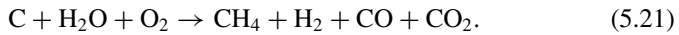


Fig. 5.22 graphically presents steam conversion for the simplest case: The initial substances include C and H_2O . The reaction products are presented by CH_4 , H_2 , and CO .

The process proved to be very sensitive to temperature variation with simultaneous change of the Gibbs energy surface shape, the thermodynamic attainability region, the position of the final equilibrium point and the extreme point, and the character of thermodynamic situation on the segment [1–2], i.e., at the transition

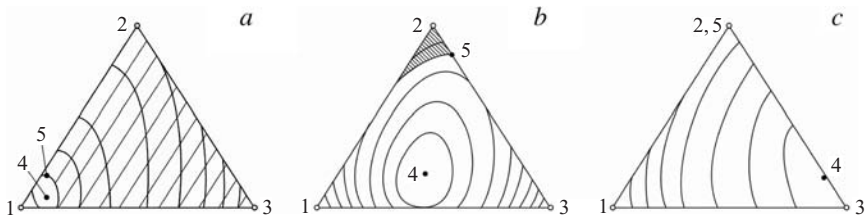


FIGURE 5.22. Steam conversion of carbon. Vertices: 1 – y : C_c , H_2O ; 2 – CH_4 ; 3 – CO , H_2 . Thermodynamic states: 4 – x^{eq} , 5 – $x_{\text{CH}_4}^{\text{ext}}$. Thermodynamic parameters: $P = 5 \text{ MPa}$; T , K: a) 700, b) 800, c) 900. The region of thermodynamic inaccessibility is hatched.

from the initial point (vertex 1) to the vertex with the maximum possible yield of CH_4 (vertex 2).

At a low temperature (<700 K) the thermodynamic attainability region is negligible (Fig. 5.22a). The points x^{eq} and $x_{\text{CH}_4}^{\text{ext}}$ lie near the vertex y . There is a thermodynamic pothole on the segment [1–2]. When the temperature rises to 800 K, $D_i(y)$ sharply increases. The point $x_{\text{CH}_4}^{\text{ext}}$ shifts to vertex 2 ($x_{\text{CH}_4}^{\text{mat}}$). The thermodynamic constraints become increasingly less strict. At $T > 900$ K they disappear. The extreme point reaches the vertex 2, i.e., the following equality is met:

$$x_{\text{CH}_4}^{\text{ext}} = x_{\text{CH}_4}^{\text{mat}}$$

The final equilibrium point shifts to the vertex 3 that corresponds to the process products H_2 and CO .

For the total system (5.21) the thermodynamic constraints are significant. The solution $x_{\text{CH}_4}^{\text{ext}}$ lies on the curve $G = G(y)$ and in the whole studied range of external parameters (change of T from 400 to 1200 K and the mole ratio $\text{O}_2:\text{C}$ from 0 to 0.5) the condition

$$x_{\text{CH}_4}^{\text{ext}} < x_{\text{CH}_4}^{\text{mat}}$$

is satisfied. Here the extreme yield is no more than 52% of the maximum possible yield subject to the material balance. This quantity determines the extent of initial carbon transition to methane (Table 5.5).

Fig. 5.23 illustrates the effect of process temperature on methane yield (at the states x^{eq} and $x_{\text{CH}_4}^{\text{ext}}$). It shows that a temperature of about 800 K is optimal for the process from the thermodynamic viewpoint. The methane yield in this case reaches 90% of the extreme yield.

Plasma Gasification

This example is interesting first of all because it deals with *high-energy chemistry* [26], which is characterized by the most crucial case of nonequilibrium—a sharp deviation in distribution of some microscopic quantity from equilibrium distribution. It is clear that the successful application of the models of equilibrium

TABLE 5.5. The extent of initial carbon conversion to methane ($P = 5$ MPa, $T = 800$ K)

Mole ratio $\text{O}_2:\text{C}$	Mole ratio $\text{H}_2\text{O}:\text{C} = 2$		Mole ratio $\text{H}_2\text{O}:\text{C} = 3$	
	x^{eq}	$x_{\text{CH}_4}^{\text{ext}}$	x^{eq}	$x_{\text{CH}_4}^{\text{ext}}$
0	0.46	0.51	0.45	0.52
0.1	0.42	0.51	0.40	0.52
0.2	0.37	0.51	0.35	0.52
0.3	0.32	0.51	0.30	0.52
0.4	0.27	0.51	0.25	0.52
0.5	0.22	0.51	0.20	0.52

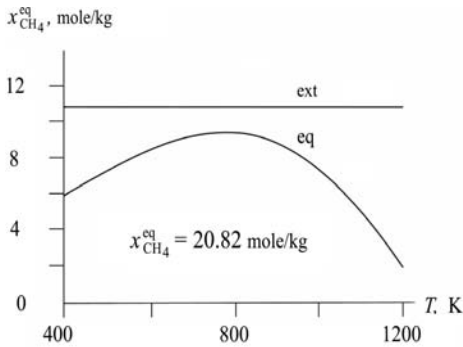


FIGURE 5.23. The equilibrium and extreme concentrations of methane versus temperature at steam conversion. $P = 5$ MPa; y , mole: 1 C, 2 H₂O.

thermodynamics in this area is an excellent illustration of the “omnipotence” of equilibrium distribution.

The use of low-temperature plasma in chemical and energy technology is attractive because an introduction of active particles (ions and free radicals) in the reaction mixture accelerates target transformations. The high-temperature jet present in the plasma reactor makes one suppose improved conditions for heat and mass exchange. Therefore, in plasma processes substantial improvements are possible for such important characteristics of chemical transformations as extent of conversion initial substances, volumetric rate of raw material supply, and selectivity. Eventually, all these factors should increase capacity of technological units, and reduce their dimensions, weight, and cost.

As an energy carrier, electricity applied in plasma generators (plasmatrons) provides high performance in plasma-chemical reactors, allowing for simplicity of start-up and load control, and high maneuverability.

Plasma processes can find possible applications in fuel gasification to produce *syngas* (a mixture of CO and H₂), gasification in the system of fuel preparation and the integrated gasification combined cycle at power plants, and ignition and lightening of the pulverized-coal torch in boiler furnaces. The latter option has already been implemented in the Russian power sector [95, 149].

Perfection limits for plasma technologies, in particular plasma gasification of coal, can be estimated using thermodynamics based on the assumptions that the intensity of exchange processes in the plasma reactor favors quick leveling of the flow temperatures, and that reactions proceed along the equilibrium trajectories.

In the first MEIS-based calculations of plasma gasifiers the authors included the *electric neutrality equation* (2.78) in the system of constraints. However, comparison of the calculation results with the data of pilot installation operation showed that the composition of final products of plasma gasification corresponded to the final equilibrium state (x^{eq}) of the ordinary gasification processes (with production of energy that was needed for the endothermal process supplied by burning an additional amount of fuel). The difference between plasma and traditional technologies is that in the latter the point x^{eq} is not reached. Therefore, condition (2.78) in thermodynamic calculations of plasma gasifiers was unnecessary.

FIGURE 5.24. The share of active species x (atoms, ions, etc.) in the plasma-forming gas versus its temperature T_{pl} . 1-CO₂; 2- H₂O; 3-H₂ or O₂.

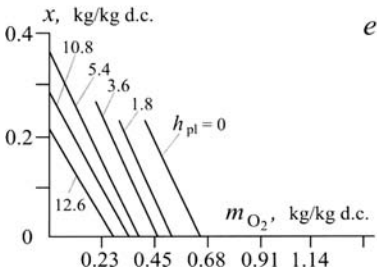
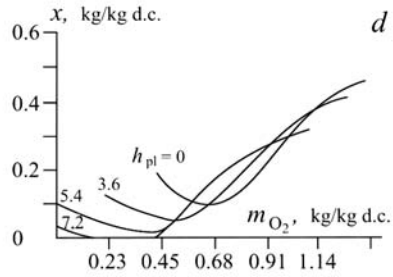
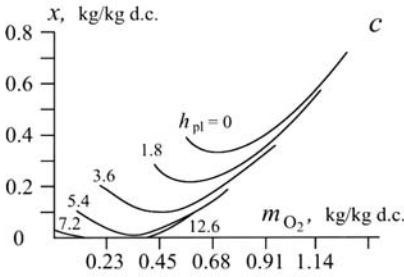
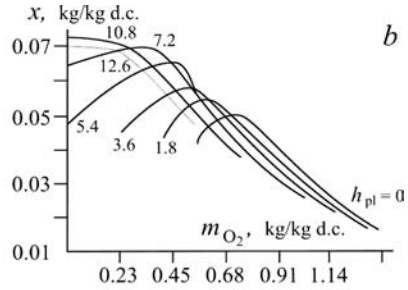
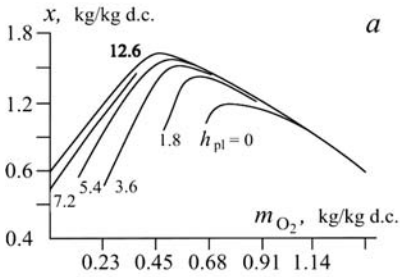
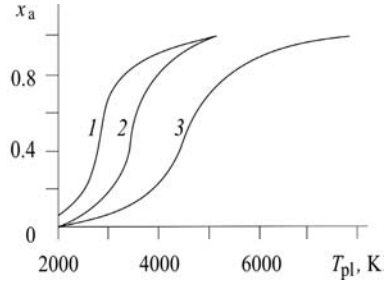


FIGURE 5.25. Plasma gasification of coal. Specific yields of (a) carbon oxide x_{CO} , (b) hydrogen x_{H_2} , (c) carbon dioxide x_{CO_2} , (d) water vapor x_{H_2O} , and (e) condensed carbon x_{C_c} as functions of oxygen consumption m_{O_2} at different plasma energy values h_{pl} , MJ/kg d.c. ($m_{H_2O} = 0.114\text{kg/kg dry coal}$).

This electric neutrality equation should obviously be included in the system of MEIS constraints at modeling the processes in plasmatrons and when choosing the plasma-forming gases.

The main plasma-forming gases in technologies of fossil fuel processing and burning may be H_2O , CO_2 , and O_2 (in some cases H_2). MEIS was applied to study their ability to ionize in the range of operation temperatures (2500–8000 K) of plasmatrons [82]. The calculation results are given in Fig. 5.24, which shows that CO_2 is ionized the most easily, H_2O is ionized with considerably more difficulty, and O_2 and H_2 are ionized most poorly. At $T = 3500$ K the quantity of active species in CO_2 plasma is 47% higher than in plasma of H_2O and 88% higher than in plasma of O_2 and H_2 ; for $T = 4500$ K these ratios make up 14% and 59%, respectively. Hence, CO_2 and H_2O are the most adequate for use as plasma-forming gases.

As in the previous examples of combustion and gasification, the perfection limits of plasma technology were calculated as applied to Kansk–Achinsk coal. In calculations the values of specific (per 1 kg of dry coal (d.c.)) consumption of water vapor, oxygen and plasma energy were varied over wide ranges. The calculations resulted in determination of dependences of process equilibrium temperature and the product specific yields (CO , H_2 , CO_2 , H_2O , etc.), as well as the dependences of efficiency on the indicated varied quantities. Some calculation results are presented in Fig. 5.25.

The thermodynamic analysis of competing coal gasification processes showed that the plasma processes are characterized by higher yields of the target products CO and H_2 and lower yields of the ballast constituents. Application of the results of thermodynamic modeling in broader technical and economic studies on plasma gasification proved that this process can be competitive when electricity consumption for plasmatrons is no more than 6–7% of the total energy (chemical and electric) consumption [82]. The current progress in plasma technologies allows us to take these figures as attainable [95, 149].